Copy 5
RM L52G08

NACA RM L52G08

NACA

RESEARCH MEMORANDUM

HINGE-MOMENT AND CONTROL-EFFECTIVENESS CHARACTERISTICS OF AN OUTBOARD FLAP WITH AN OVERHANG NOSE BALANCE ON A TAPERED 35° SWEPTBACK WING OF ASPECT RATIO 4

TRANSONIC-BUMP METHOD

By Robert F. Thompson and William C. Moseley, Jr.

Langley Aeronautical Laboratory
Langley Field, Va.

NATIONAL ADVISORY COMMITTEE FOR AERONAUTICS

WASHINGTON
August 28, 1952

1D

NACA RM L52G08

NATIONAL ADVISORY COMMITTEE FOR AERONAUTICS

RESEARCH MEMORANDUM

HINGE-MOMENT AND CONTROL-EFFECTIVENESS CHARACTERISTICS OF AN OUTBOARD FLAP WITH AN OVERHANG NOSE BALANCE ON A TAPERED 35° SWEPTBACK WING OF ASPECT RATIO 4

TRANSONIC-BUMP METHOD

By Robert F. Thompson and William C. Moseley, Jr.

SUMMARY

An investigation was made in the Langley high-speed 7- by 10-foot tunnel to determine the hinge-moment and control-effectiveness characteristics of a tapered, 35° sweptback, semispan wing equipped with an outboard 43-percent-span flap. The wing had an aspect ratio of 4, a taper ratio of 0.6, an NACA 65A006 airfoil section parallel to the free stream, and was tested through a Mach number range of 0.60 to 1.10.

The hinge-moment parameters C_{h_δ} and C_{h_α} were negative throughout the speed range and showed a large negative increase in the speed range from a Mach number of approximately 0.90 to a Mach number of 1.00. There was a pronounced decrease in the control-effectiveness parameters in the Mach number range from about 0.80 to 1.00.

INTRODUCTION

A transonic research program was established by the National Advisory Committee for Aeronautics whereby a series of wing-body configurations having wing plan form as the chief geometric variable were investigated. As part of this program a wing having 35° sweepback of the quarter chord line was tested in the Langley high-speed 7- by 10-foot tunnel with and without trailing-edge flaps (refs. 1 and 2).

The primary purpose of the present investigation was to obtain experimental hinge-moment data for a flap-type control at transonic

speeds. A 43-percent-span outboard flap-type control having a 22-percent-flap-chord overhang nose balance was tested on a wing geometrically similar to but slightly larger than the wing used in references 1 and 2. In addition to the hinge moments, the lift, rolling-moment, and pitching-moment characteristics of the wing-control configuration were determined. Results are given for a range of flap deflections at angles of attack from -6° to 16° and through a Mach number range from 0.6 to 1.10.

COEFFICIENTS AND SYMBOLS

C_h	flap hinge-moment coefficient, $H/q2M'$
H	flap hinge moment measured about hinge line, ft-lb
C_L	lift coefficient, Twice lift of semispan model/qS
M'	area moment of the flap back of the hinge line, 0.000380 ft^3
C_l	rolling-moment coefficient at plane of symmetry, Rolling moment of semispan model/qSb
C_m	pitching-moment coefficient referred to $0.25\bar{c}$, Twice pitching moment of semispan model/$qS\bar{c}$
q	effective dynamic pressure over span of model, $\frac{\rho V^2}{2}$, lb/sq ft
S	twice wing area of semispan model, 0.250 sq ft
b	twice span of semispan model, 1.000 ft
$\bar{c}$	mean aerodynamic chord of wing, 0.255 ft, based on relationship $\frac{2}{S}\int_0^{b/2} c^2 dy$ (using theoretical tip)
c	local wing chord, ft
c_f	flap chord, ft
y	spanwise distance from plane of symmetry, ft
ρ	mass density of air, slugs/cu ft
V	free-stream air velocity, ft/sec

[redacted]

M effective Mach number over span of model, $\frac{2}{S}\int_0^{b/2} cM_a dy$

M_a average chordwise local Mach number

M_l local Mach number

A aspect ratio, $\frac{b^2}{S}$

R Reynolds number of wing based on $\bar{c}$

α angle of attack, deg

δ control-surface deflection, measured in a plane perpendicular to control-surface hinge line, positive when control-surface trailing edge is below wing-chord plane, deg

λ taper ratio (Tip chord/Root chord)

$$C_{L_\delta} = \left(\frac{\partial C_L}{\partial \delta}\right)_\alpha$$

$$C_{l_\delta} = \left(\frac{\partial C_l}{\partial \delta}\right)_\alpha$$

$$C_{m_\delta} = \left(\frac{\partial C_m}{\partial \delta}\right)_\alpha$$

$$C_{h_\delta} = \left(\frac{\partial C_h}{\partial \delta}\right)_\alpha$$

$$C_{h_\alpha} = \left(\frac{\partial C_h}{\partial \alpha}\right)_\delta$$

The subscript outside the parentheses indicates the factor held constant during the measurement of the parameters.

MODEL AND APPARATUS

The steel semispan wing had 35° sweepback of the quarter chord line, an aspect ratio of 4, a taper ratio of 0.6, and an NACA 65A006 airfoil section measured parallel to the free stream. A drawing of the wing giving pertinent dimensions and data is shown in figure 1.

[redacted]

The wing was equipped with a trailing-edge flap-type control hinged at the 0.70 chord line. The flap was constructed by glueing spruce to a steel spar and was mass-balanced by a lead overhang nose balance. The nose balance, elliptical in shape, was 22 percent of the flap chord and its size was determined primarily because of the necessity of mass balancing the flap to alleviate the possibility of coupled wing-flap flutter. The flap was located at the outboard portion of the wing and had a span equal to 0.43 wing semispan. The flap was hinged to the wing with a hinge pin at the wing tip and a hinge rod passing through the wing along the 70-percent chord line to the chamber within the bump. The gap between the wing and flap was about 0.05 flap chord (0.015c), and was left unsealed for these tests. Flap hinge moments were measured by a calibrated beam-type electric strain gage fastened rigidly to the hinge rod below the bump surface.

The model was mounted on an electrical strain-gage balance and the aerodynamic forces and moments were recorded by means of calibrated potentiometers. The balance was mounted in a sealed chamber within the bump. The model butt passed through a hole in the turntable in the bump surface. Leakage through this hole was kept to a minimum by the use of a sponge-wiper seal fastened to the undersurface of the bump turntable.

TESTS

The tests were made in the Langley high-speed 7- by 10-foot tunnel by utilizing the transonic-bump technique. This technique involved the mounting of the model in the high-velocity flow field generated over the curved surface of a bump located on the tunnel floor.

Typical contours of local Mach number in the vicinity of the model location on the bump, obtained with no model in position, are shown in figure 2. The effective Mach number over the wing semispan was generally slightly higher than the effective Mach number over that portion of the wing where the flap was located. The long dashed line shown near the root chord indicates a local Mach number that is 5 percent below the maximum value and represents the extent of the boundary layer. The effective test Mach numbers were obtained from contour charts similar to those of figure 2 by using the relationship

$$M = \frac{2}{S}\int_0^{b/2} cM_a dy$$

[redacted]

The variation of Reynolds number with Mach number for typical test conditions is presented in figure 3. The Reynolds numbers were based on a mean aerodynamic chord of 0.255 foot. Lift, rolling moment, pitching moment, and hinge moment were obtained through a Mach number range of 0.60 to 1.10, an angle-of-attack range of -6° to 16°, and for a range of flap deflections which varied from about $\pm 24^\circ$ at the low Mach numbers to $\pm 12^\circ$ at the higher Mach numbers.

CORRECTIONS

No corrections have been applied to the data for the chordwise and spanwise velocity gradients or for distortion of the wing due to air loads, but these corrections are believed to be small. Flap deflections have been corrected for twisting of the long hinge rod of small diameter between the hinge-moment strain gage and the flap. (See fig. 1.) Flap-deflection corrections were determined from a static hinge-moment calibration and applied according to the measured test hinge moment. This correction was large and for the extreme loading condition was about 65 percent of the original flap setting. Despite the large values of applied flap-deflection correction, the final flap deflections are believed to be reliable since care was taken not to exceed the proportional limit of the hinge rod, and the control-effectiveness parameters compare very well with previously published data on a similar configuration having a comparatively rigid flap.

No reflection-plane corrections have been applied to the data for the rolling-moment coefficient against δ but C_{l_δ} given in this paper has been corrected by the reflection-plane correction factor given in reference 2. This correction was obtained from unpublished experimental corrections obtained at low speed ($M = 0.25$) and theoretical considerations. Although the corrections are based on incompressible conditions and are only valid for low Mach numbers, they were applied throughout the Mach number range in order to give a better representation of true conditions than would be shown by the uncorrected data. For the configuration of the present investigation the correction was applied as follows:

$$C_{l_\delta} = \left(C_{l_\delta}\right)_{\text{measured}} - 0.13\left(C_{l_\delta}\right)_{\text{measured}}$$

The lift and pitching-moment data represent the aerodynamic effects that would be obtained on a complete wing with both control surfaces deflected in the same direction and therefore no reflection-plane corrections are necessary.

RESULTS AND DISCUSSION

Presentation of Data

The variation of C_h with flap deflection for the various angles of attack is presented through the Mach number range in figure 4. The plot of C_h against α for $\delta = 0^\circ$ is given for the test Mach numbers in figure 5. The variations of the aerodynamic coefficients C_L, C_l, and C_m with flap deflection for the test angles of attack are presented for the various Mach numbers as figures 6, 7, and 8, respectively. The effect of Mach number on the hinge-moment parameters C_{h_δ} and C_{h_α} is given in figure 9. Figure 10 shows the variation of C_{L_δ}, C_{l_δ}, and C_{m_δ} with Mach number and compares these results with similar results from reference 2.

Hinge-Moment Characteristics

The variation of hinge-moment coefficient with flap deflection is shown in figure 4. The slope of C_h with δ is negative for all test conditions except for high negative deflections at angles of attack greater than 8° in the Mach number range from 0.80 to 0.95 where the slope became marginal or in some cases positive. Increasing the Mach number above $M = 0.95$ eliminated this slope reversal.

A plot of hinge-moment coefficient against angle of attack at $\delta = 0^\circ$ is presented in figure 5. No test data points were plotted on this figure since, because of the hinge-rod-deflection correction, it was necessary to crossplot the data to obtain values of C_h at $\delta = 0^\circ$. The curve for C_h against α at $\delta = 0^\circ$ is linear over a range of angle of attack of $\pm 6^\circ$ from $M = 0.6$ to $M = 0.95$ and becomes linear over a larger angle-of-attack range as the Mach number is increased above $M = 0.95$.

The effect of Mach number on the hinge-moment parameters C_{h_δ} and C_{h_α} is shown in figure 9. The parameter C_{h_δ} was measured at $\alpha = 0^\circ$ over a δ range of at least $\pm 6^\circ$ where the curves were linear. The value of C_{h_δ} is negative throughout the Mach number range and does not vary with Mach number from $M = 0.6$ to $M = 0.8$. Above $M = 0.8$ there is a large increase in control heaviness until supersonic Mach numbers are reached where the values of C_{h_δ} are roughly 2.5 times the subsonic values. This variation of C_{h_δ} with Mach number is in agreement with the results for the full-span flaps of references 3 and 4 and the 50-percent-span outboard flap (trailing-edge angle of 7.8°) of reference 5.

[redacted]

The hinge-moment parameter C_{h_α} was measured at $\delta = 0^\circ$ over an α range of at least $\pm 6^\circ$ where the curves were linear and was negative throughout the Mach number range. The parameter C_{h_α} became less negative with Mach number up to $M = 0.9$ and then rapidly increased negatively until supersonic Mach numbers were reached where the values of C_{h_α} were roughly three times the subsonic values. This moderate decrease in negative floating tendency with Mach number up to $M = 0.9$ is in good agreement with results obtained on a full-span, radius-nose flap at higher Reynolds numbers presented in reference 6. The general variation of C_{h_α} with Mach number agrees fairly well with references 3 to 5.

Lift, Rolling-Moment, and Pitching-Moment Characteristics

The variation of lift, rolling-moment, and pitching-moment coefficient with flap deflection for the angle of attack and Mach number ranges tested is presented in figures 6, 7, and 8, respectively. The effect of Mach number on the control-effectiveness parameters C_{L_δ}, C_{l_δ} and C_{m_δ} is shown in figure 10. These parameters were measured at $\alpha = 0^\circ$ over a deflection range of at least $\pm 8^\circ$ where the curves were linear and are compared with the results of reference 2 which contains data on a flap of the same span and chord on a wing of the same plan form as the one for the present investigation. The flap of reference 2, however, was deflected by bending about the hinge line and therefore had no overhang nose or gap. The present investigation is also at a slightly higher Reynolds number mainly because of an increase in model size.

The flap was effective in producing changes in C_L, C_l, and C_m except in the high positive angle-of-attack range from $M = 0.7$ to $M = 0.95$ when a negative increase in flap deflection above about -20° resulted in a decrease in effectiveness. At Mach numbers above $M = 0.95$ the flap was effective in producing increments in C_L, C_l, and C_m throughout the α and δ range investigated.

A marked decrease in C_{L_δ} and C_{l_δ} occurred between Mach numbers of approximately 0.80 and 1.00 and a relatively smaller decrease in negative values of C_{m_δ} occurred in about the same Mach number range (fig. 10). These results (fig. 10) compare very favorably with those of reference 2. The parameters for the present investigation are slightly less in magnitude throughout the Mach number range. This decrease in flap effectiveness agrees with results obtained at low speed ($M = 0.09$) in references 7 and 8 where a flap having an elliptical $0.35c_f$ overhang nose and an unsealed gap gave lower flap effectiveness than a plain sealed flap having the same flap chord.

[redacted]

CONCLUSIONS

The results of the investigation of a tapered, 35° sweptback, semispan wing equipped with an outboard 43-percent-span flap-type control surface having a 22-percent-flap-chord overhang nose balance indicated the following conclusions:

1. The hinge-moment parameters C_{h_δ} and C_{h_α} were negative throughout the speed range and had a large negative increase in the Mach number range from approximately 0.90 to 1.00.

2. The control was effective in producing increments in lift, rolling moment, and pitching moment for all test conditions except in the high positive angle-of-attack range from a Mach number of 0.7 to a Mach number of 0.95, when a negative increase in flap deflection above about -20° did not give any increase in effectiveness. The effectiveness of the control showed a marked decrease in the Mach number range from approximately 0.80 to 1.00.

Langley Aeronautical Laboratory
National Advisory Committee for Aeronautics
Langley Field, Va.

[redacted]

REFERENCES

1. Sleeman, William C., Jr., and Becht, Robert E.: Aerodynamic Characteristics of a Wing With Quarter-Chord Line Swept Back 35°, Aspect Ratio 4, Taper Ratio 0.6, and NACA 65A006 Airfoil Section. Transonic-Bump Method. NACA RM L9B25, 1949.

2. Thompson, Robert F.: Lateral-Control Investigation of Flap-Type Controls on a Wing With Quarter-Chord Line Swept Back 35°, Aspect Ratio 4, Taper Ratio 0.6, and NACA 65A006 Airfoil Section. Transonic-Bump Method. NACA RM L9L12a, 1950.

3. Johnson, Harold I., and Goodman, Harold R.: Measurements of Aerodynamic Characteristics of a 35° Sweptback NACA 65-009 Airfoil Model With $\frac{1}{4}$-Chord Flap Having a 31-Percent-Flap-Chord Overhang Balance by the NACA Wing-Flow Method. NACA RM L50H09, 1950.

4. Lockwood, Vernard E., and Fikes, Joseph E.: Aerodynamic Characteristics at Transonic Speeds of a Tapered 45° Sweptback Wing of Aspect Ratio 3 Having a Full-Span Flap-Type Control. Transonic-Bump Method. NACA RM L51F06a, 1951.

5. Thompson, Robert F.: Investigation of a 42.7° Sweptback Wing Model To Determine the Effects of Trailing-Edge Thickness on the Aileron Hinge-Moment and Flutter Characteristics at Transonic Speeds. NACA RM L50J06, 1950.

6. Johnson, Harold S., and Thompson, Robert F.: Investigation at High Subsonic Speeds of a 45° Sweptback Horizontal Tail With Plain and Horn-Balanced Control Surfaces. NACA RM L50B13, 1950.

7. Riebe, John M., and McKinney, Elizabeth G.: Wind-Tunnel Investigation of Control-Surface Characteristics. XXII - Medium and Large Aerodynamic Balances of Two Nose Shapes and a Plain Overhang Used With a 0.20-Airfoil-Chord Flap on an NACA 0009 Airfoil. NACA ARR L5F06, 1945.

8. Riebe, John M., and Church, Oleta: Wind-Tunnel Investigation of Control-Surface Characteristics. XXI - Medium and Large Aerodynamic Balances of Two Nose Shapes and a Plain Overhang Used With a 0.40-Airfoil-Chord Flap on an NACA 0009 Airfoil. NACA ARR L5G01, 1945.

[redacted]

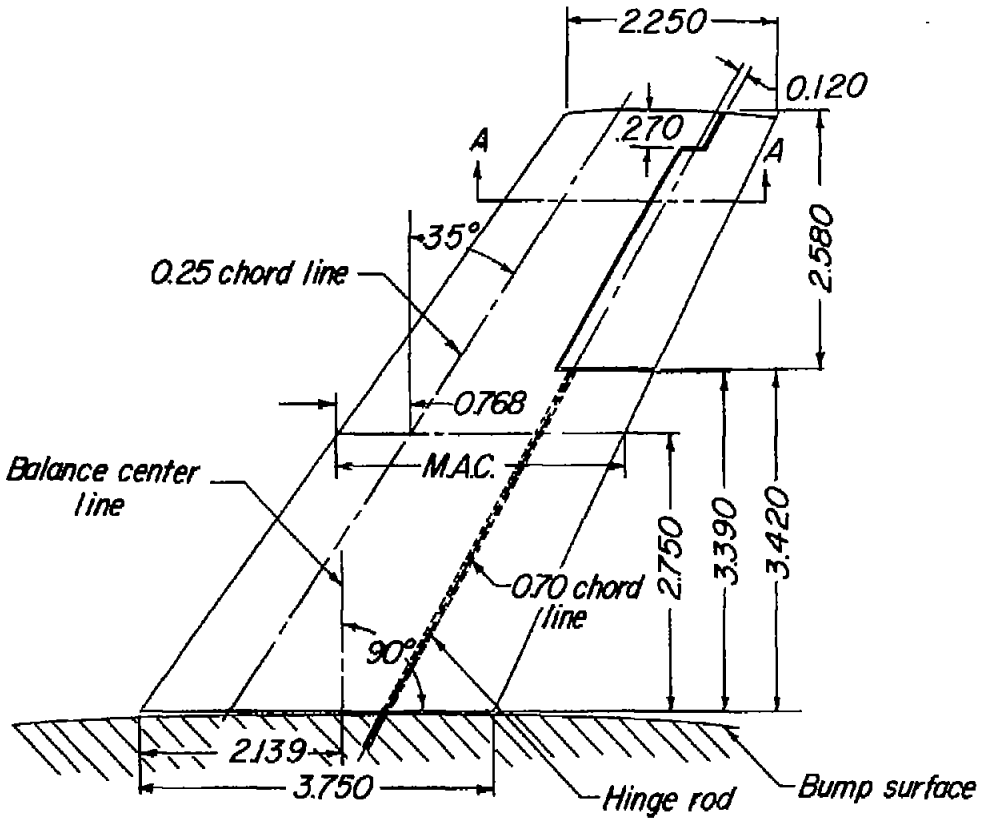

TABULATED WING DATA

Twice semispan area	0.250 sq ft
Aspect ratio	4.0
Taper ratio	0.60
Mean aerodynamic chord	0.255 ft
Airfoil section parallel to free airstream	65A006

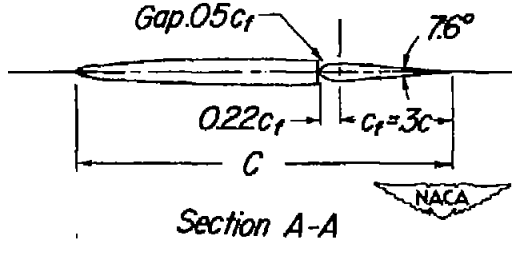

Section A-A

Figure 1.- General arrangement of the model used during the present investigation. All dimensions are in inches.

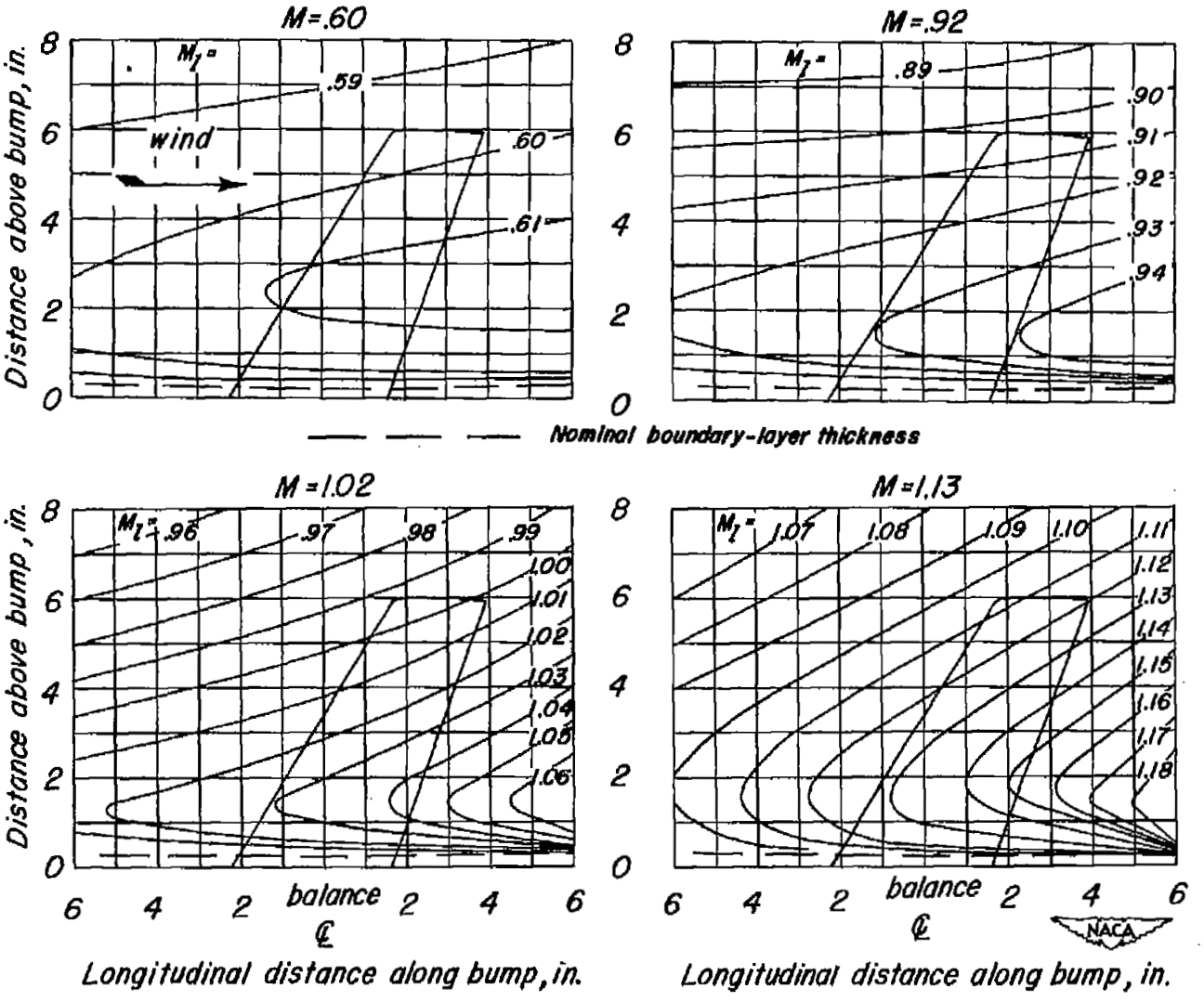

Figure 2.- Typical Mach number contours over transonic bump in region of model location.

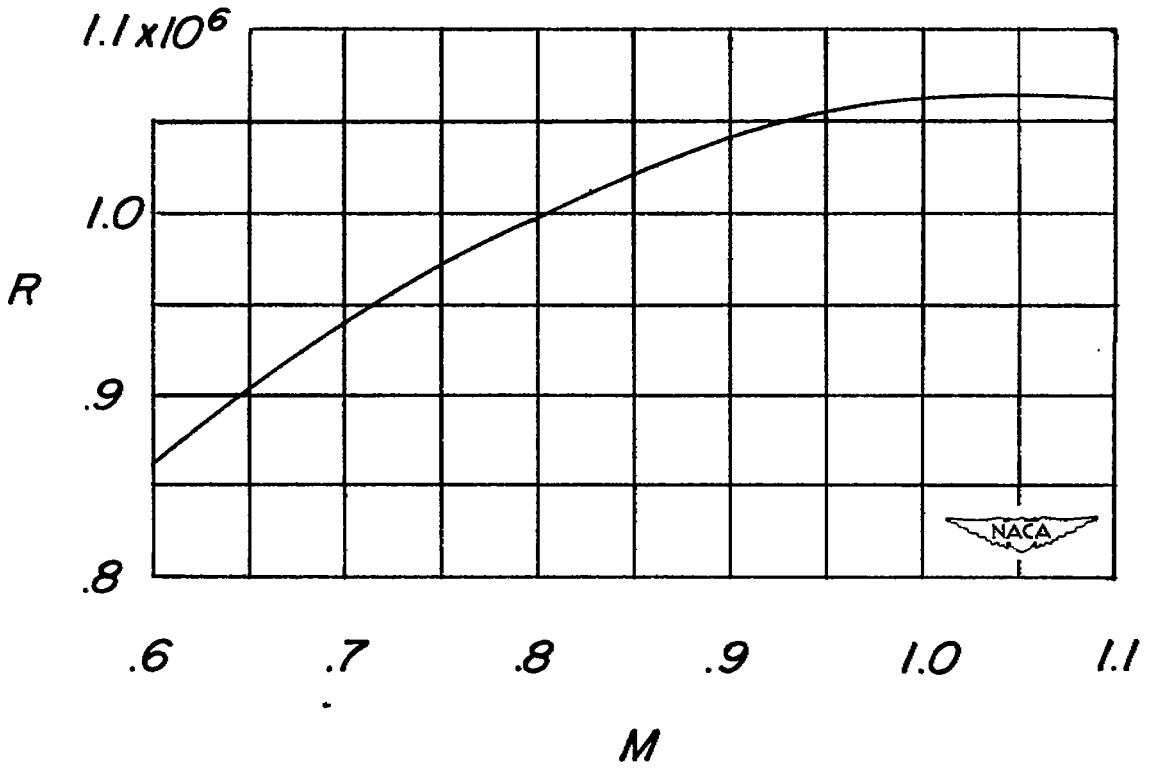

Figure 3.- Typical variation of Reynolds number with Mach number through the transonic speed range.

[redacted]

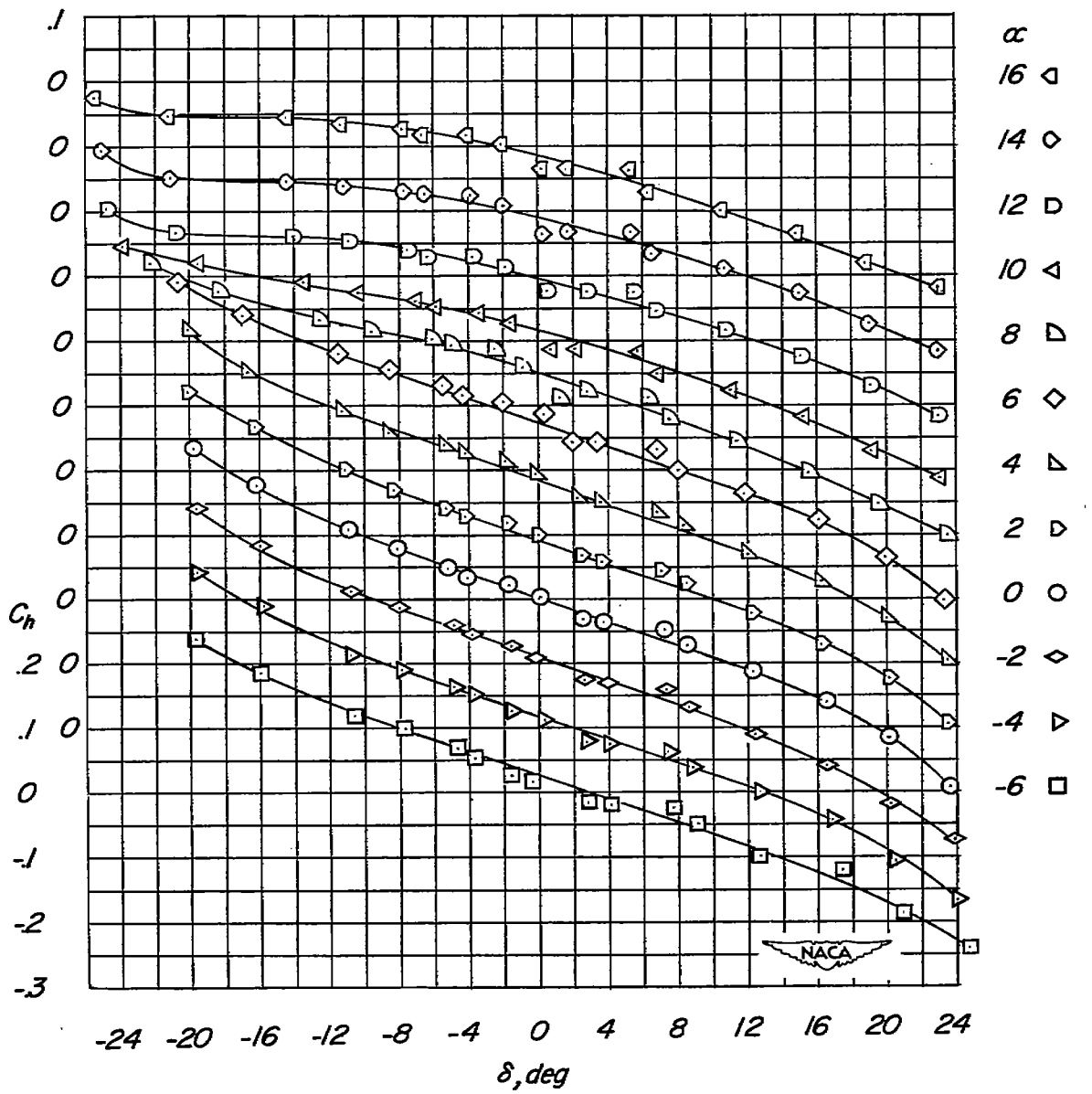

(a) M = 0.60.

Figure 4.- Variation of hinge-moment coefficient with control deflection for various angles of attack.

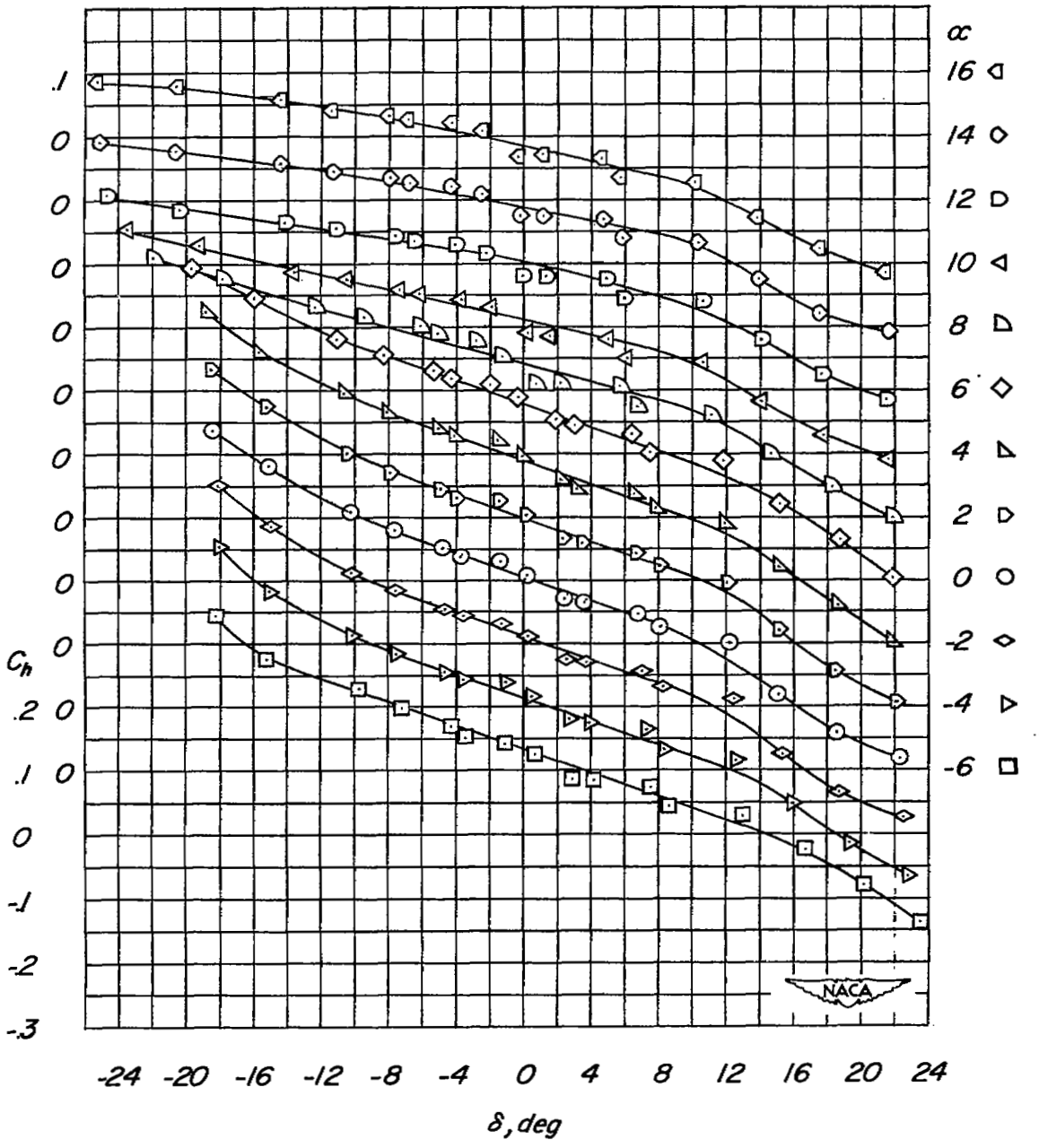

(b) M = 0.70.

Figure 4.- Continued.

[redacted]

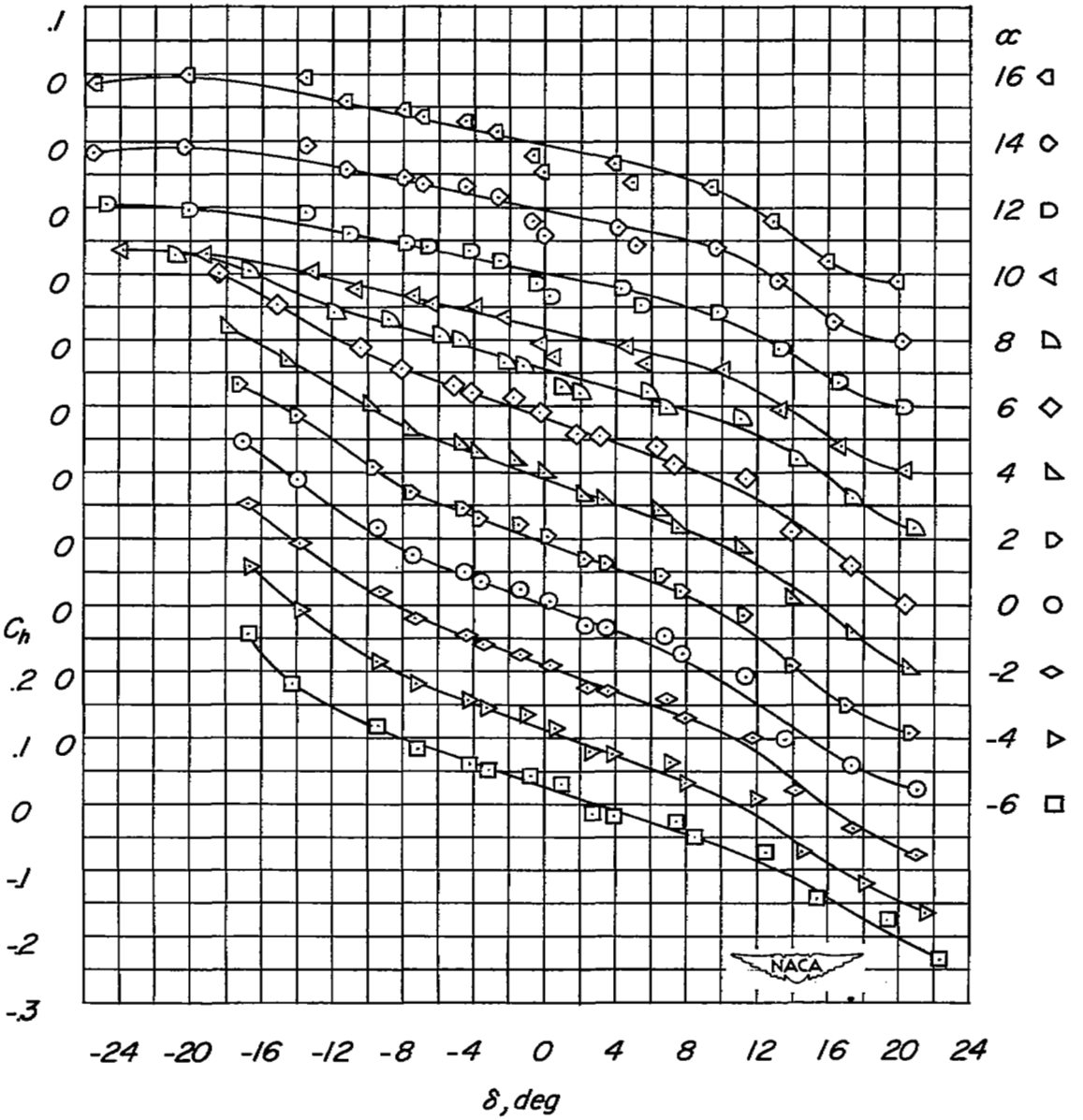

(c) M = 0.80.

Figure 4.- Continued.

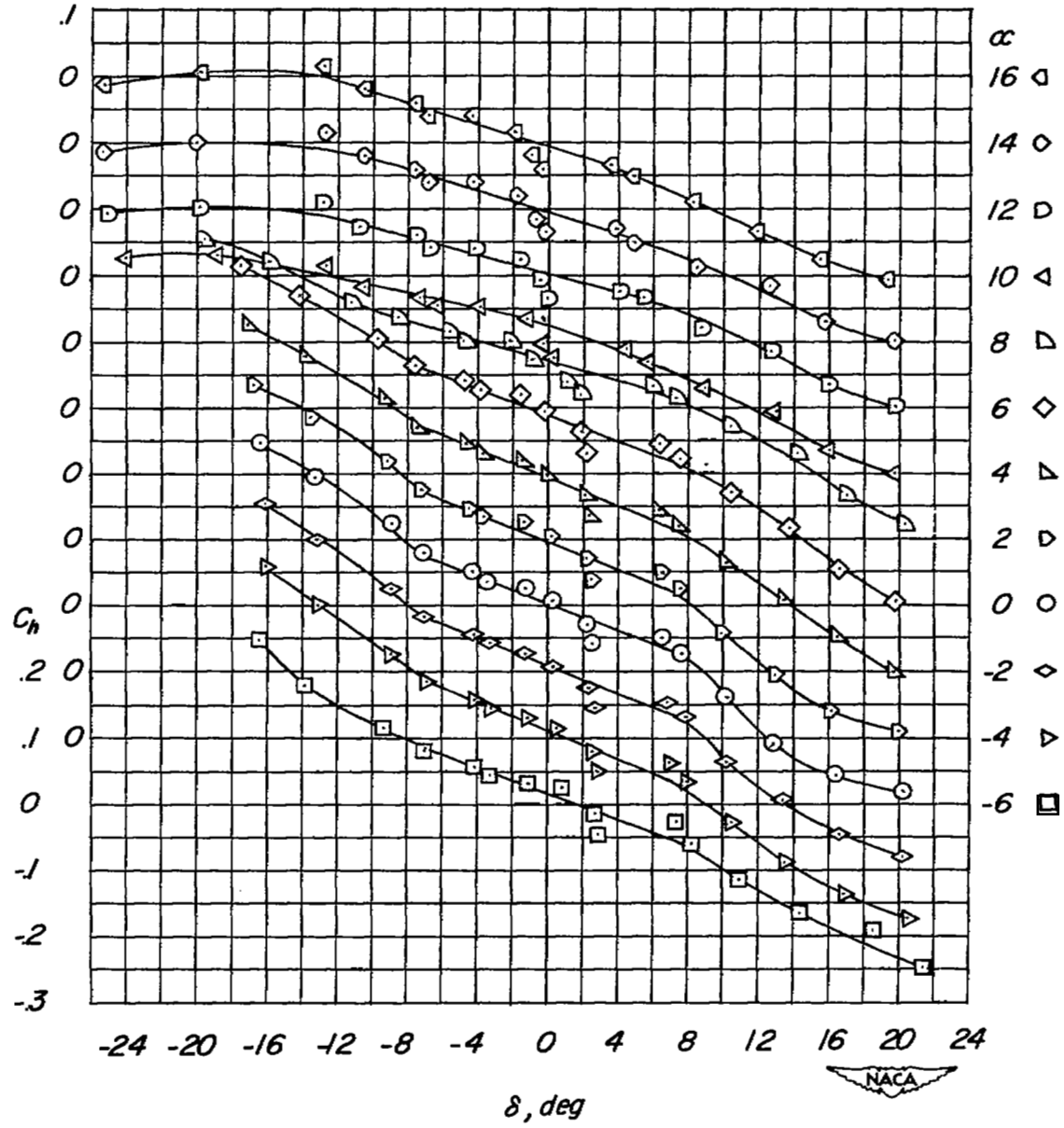

(d) M = 0.85.

Figure 4.- Continued.

[redacted]

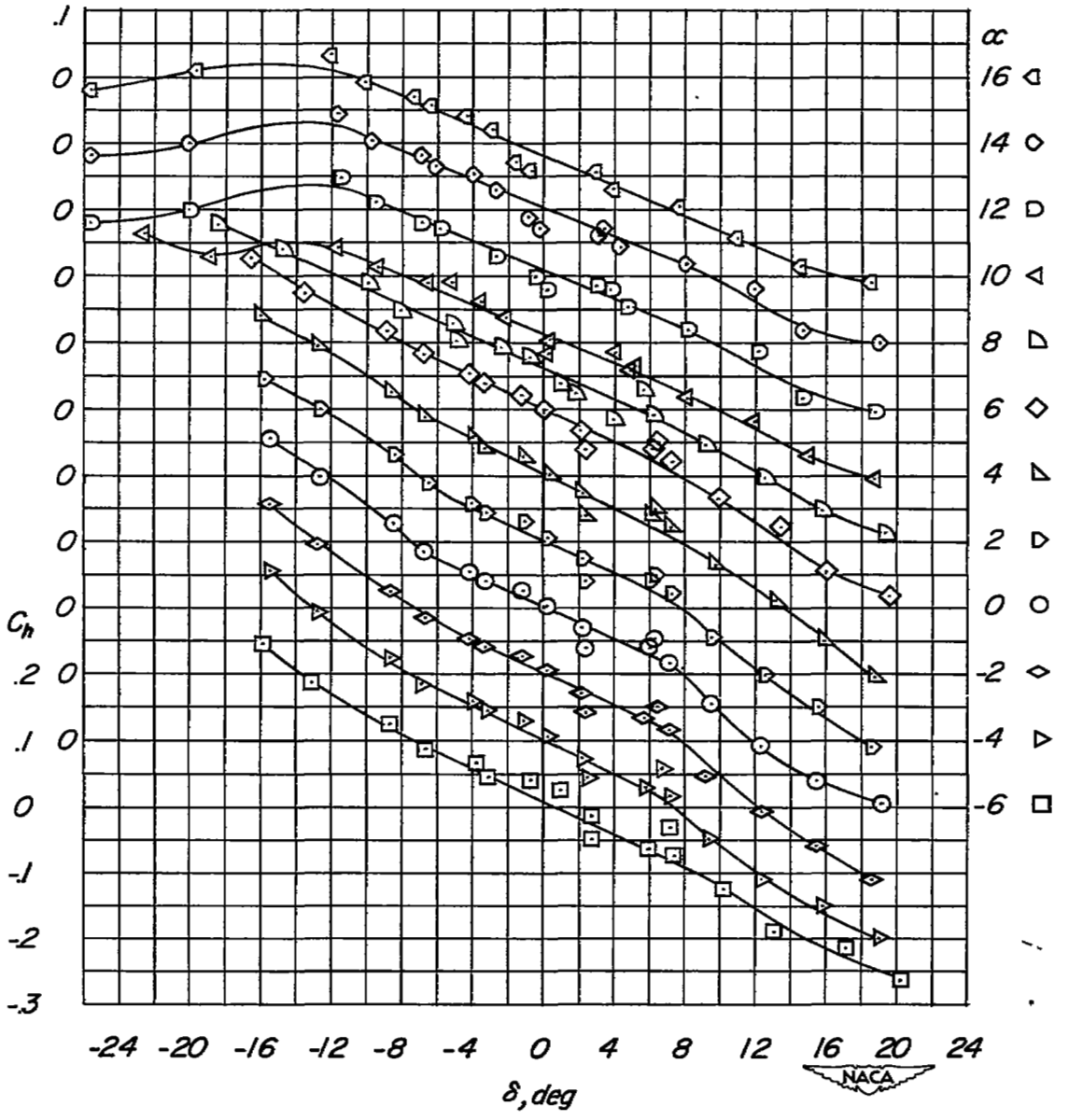

(e) M = 0.90.

Figure 4.- Continued.

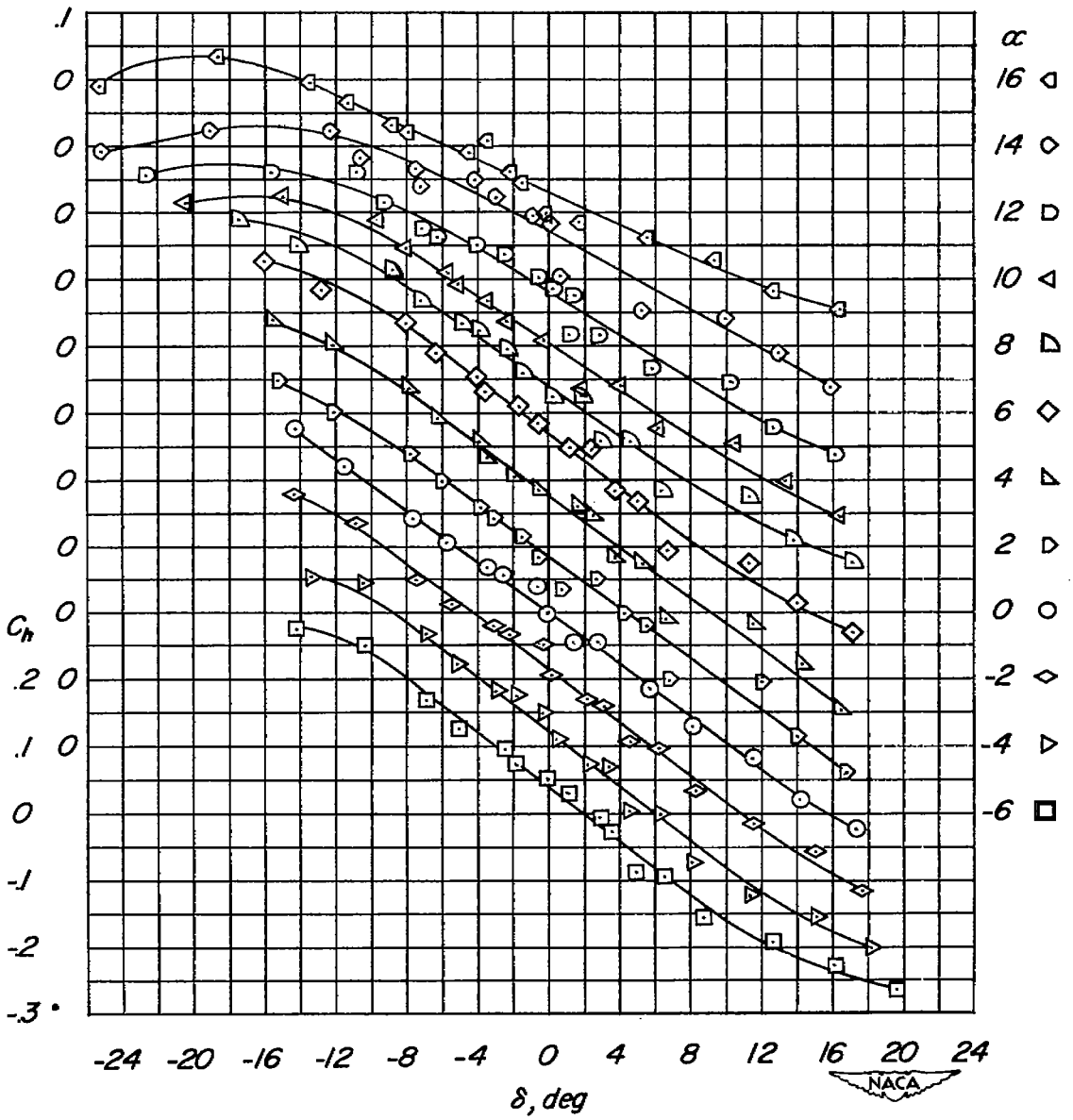

(f) M = 0.95.

Figure 4.- Continued.

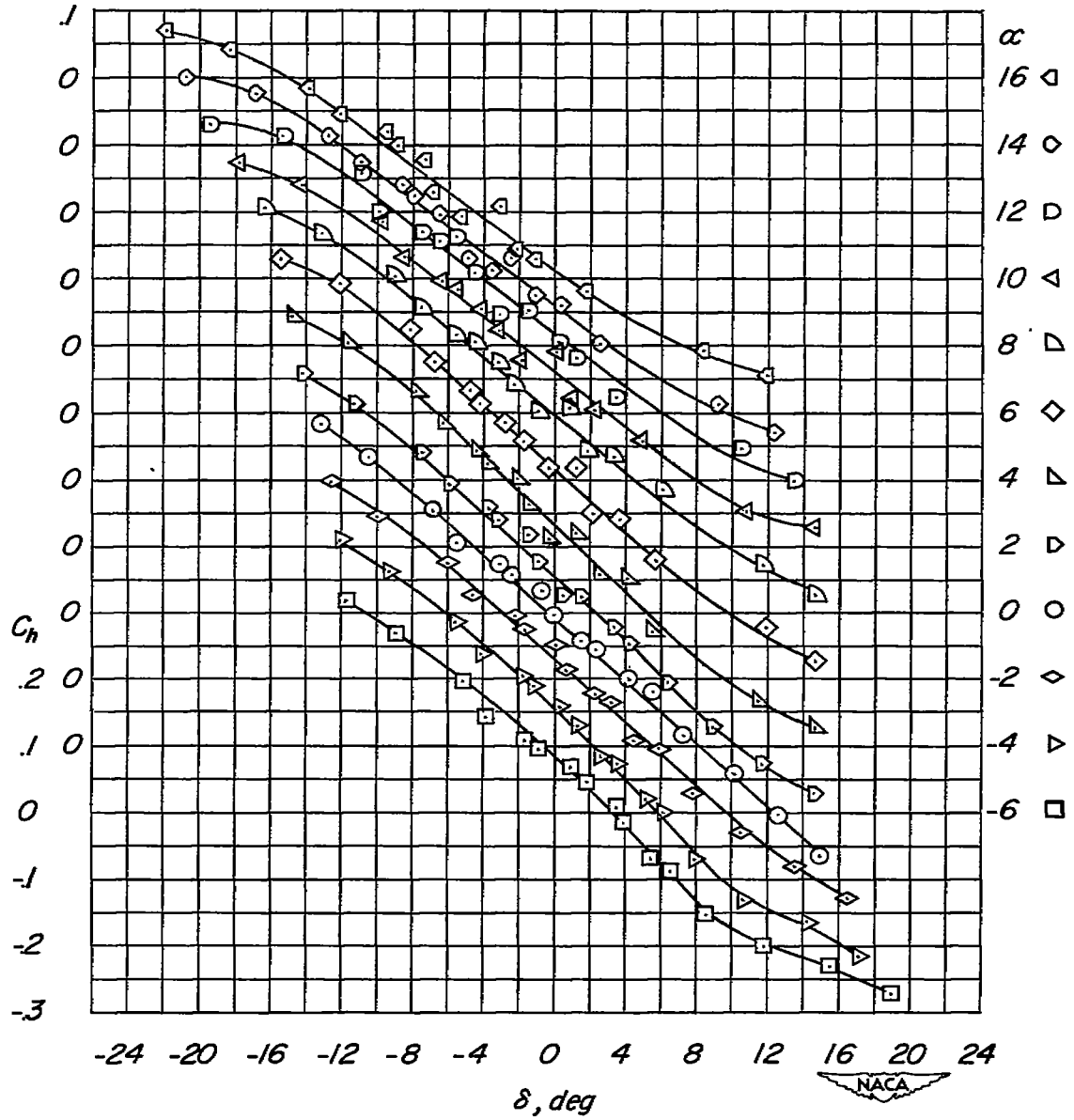

(g) M = 1.00.

Figure 4.- Continued.

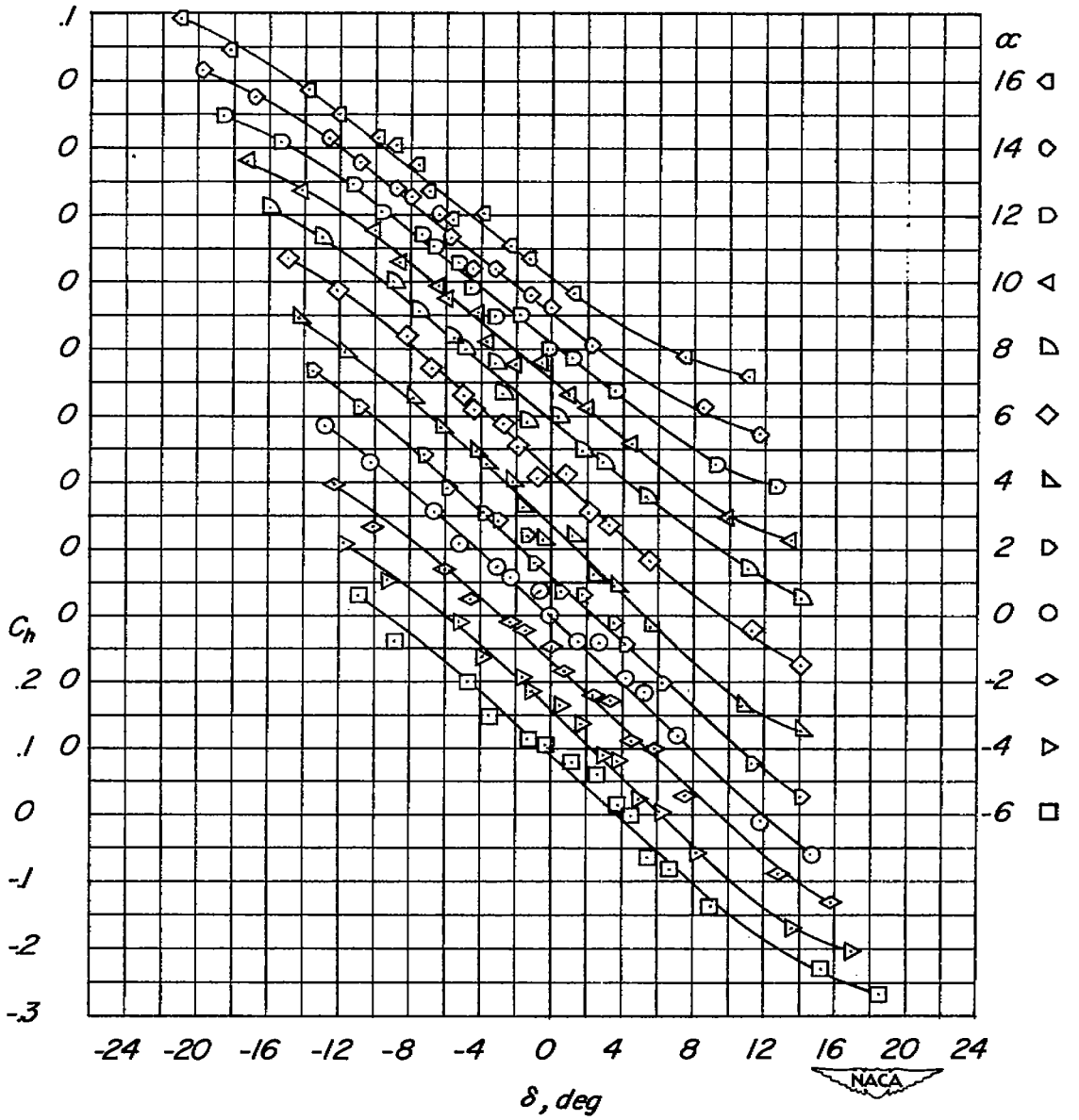

(h) M = 1.05.

Figure 4.- Continued.

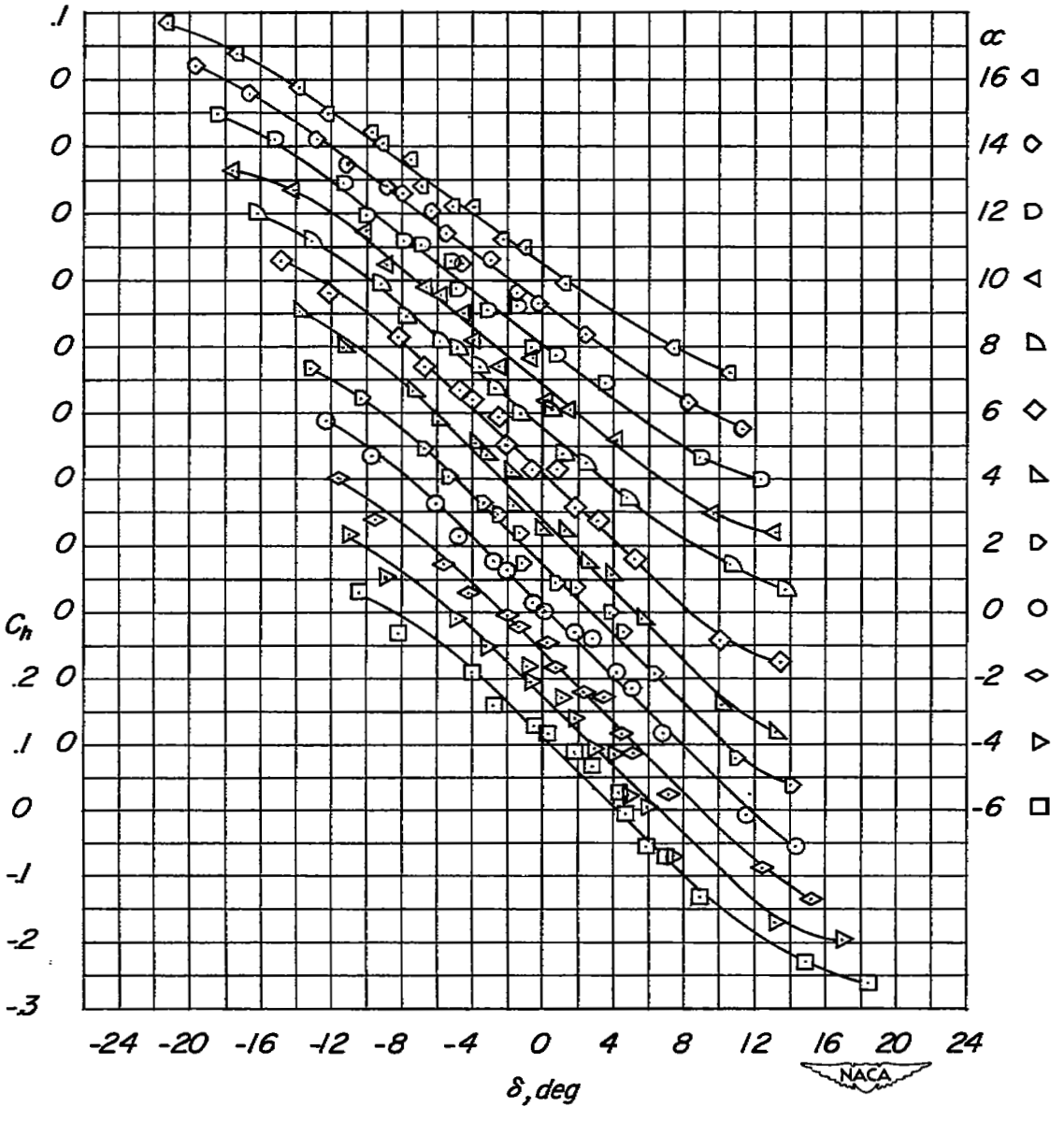

(i) M = 1.10.

Figure 4.- Concluded.

[redacted]

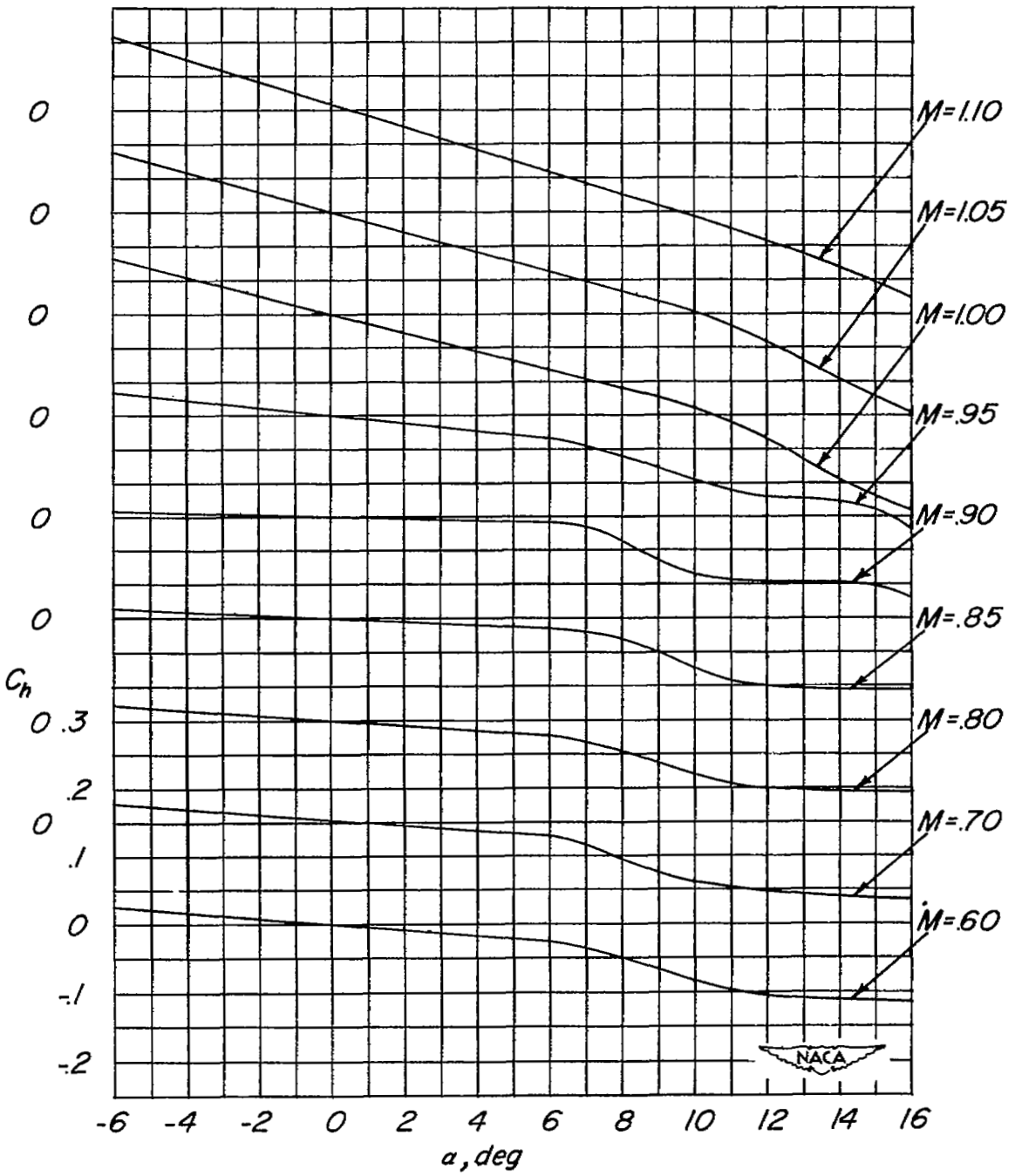

Figure 5.- Variation of hinge-moment coefficient with angle of attack for various Mach numbers. $\delta = 0$.

[redacted]

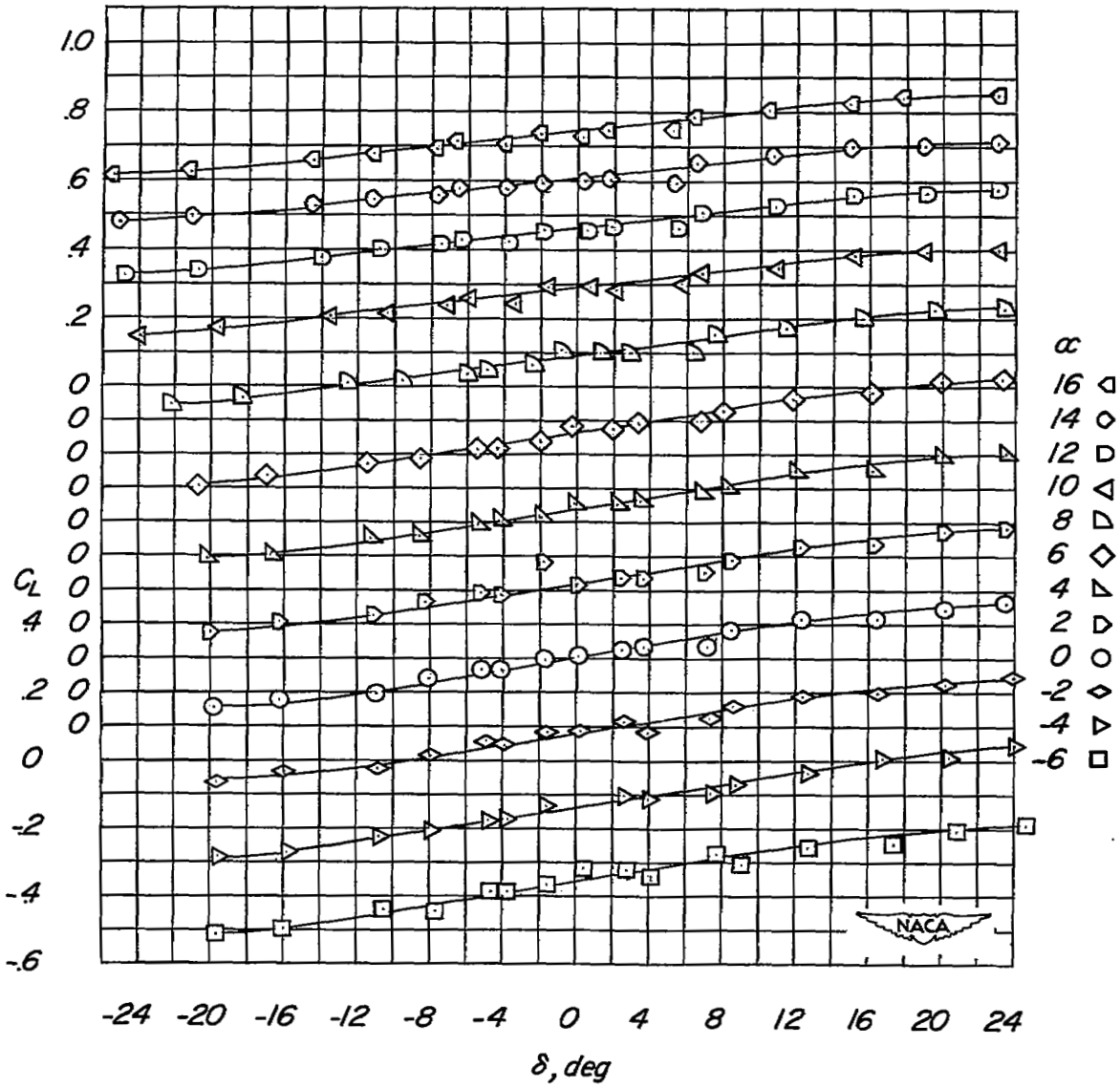

(a) M = 0.60.

Figure 6.- Variation of lift coefficient with control deflection for various angles of attack.

[redacted]

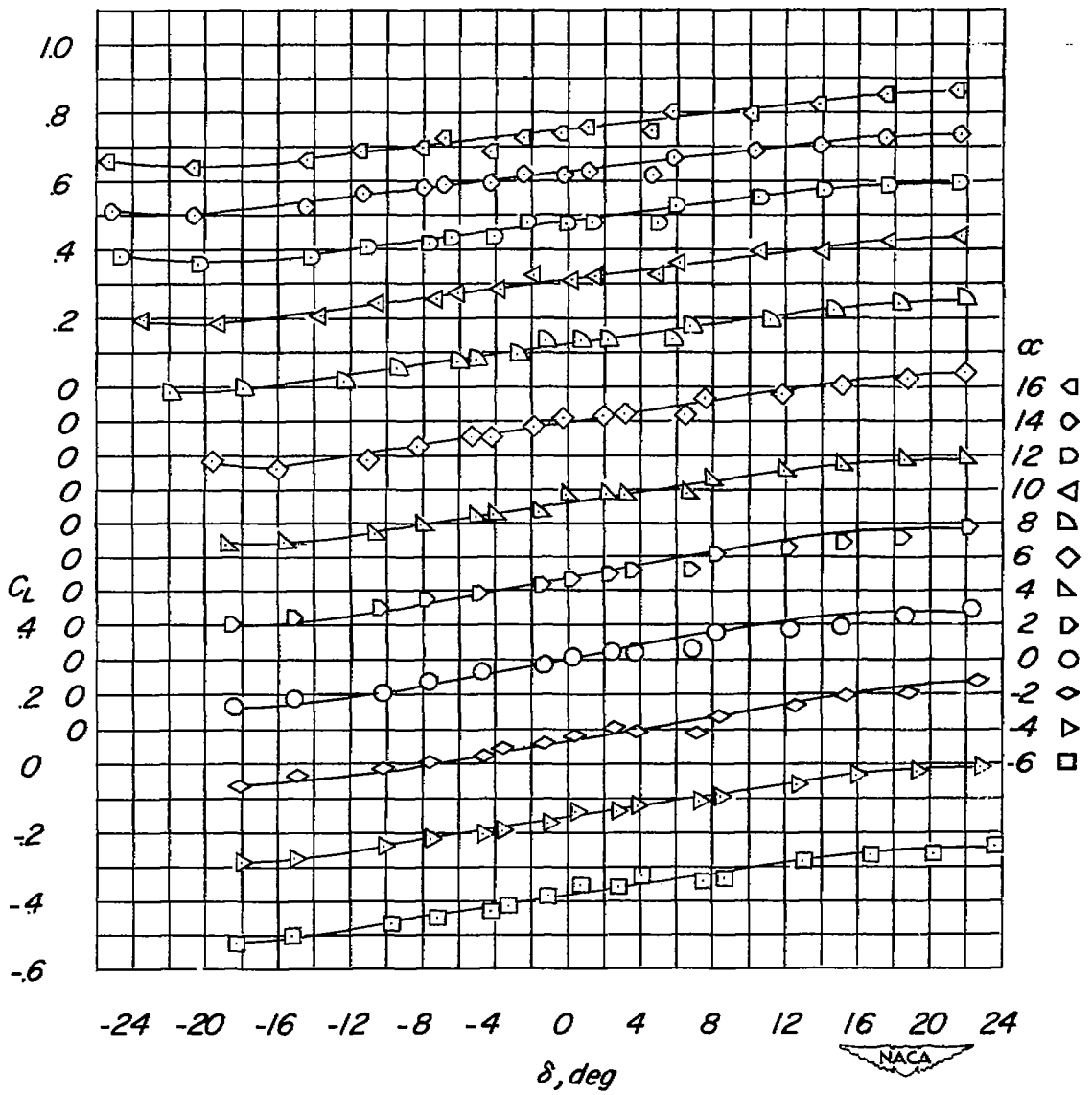

(b) M = 0.70.

Figure 6.- Continued.

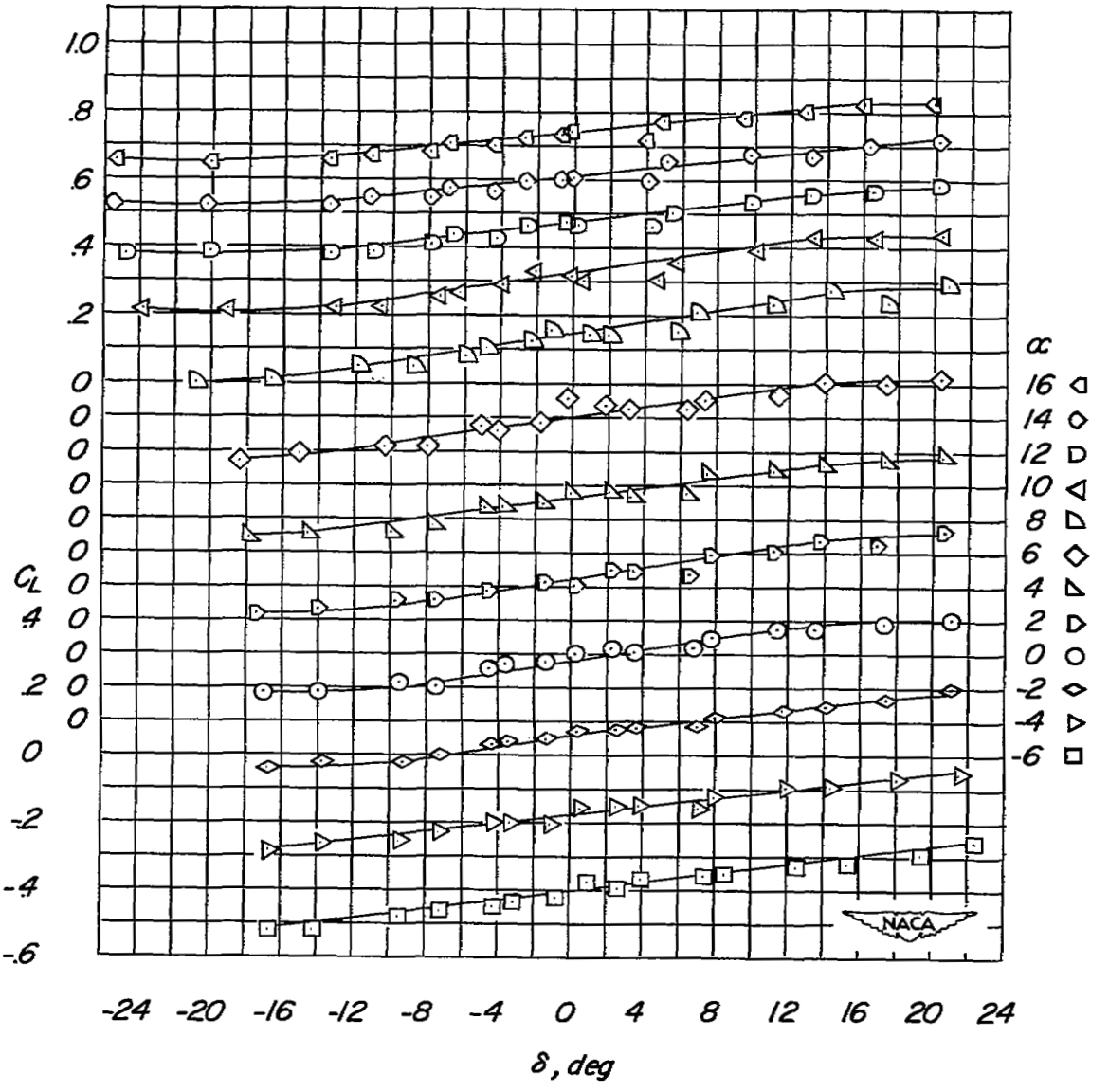

(c) M = 0.80.

Figure 6.- Continued.

[redacted]

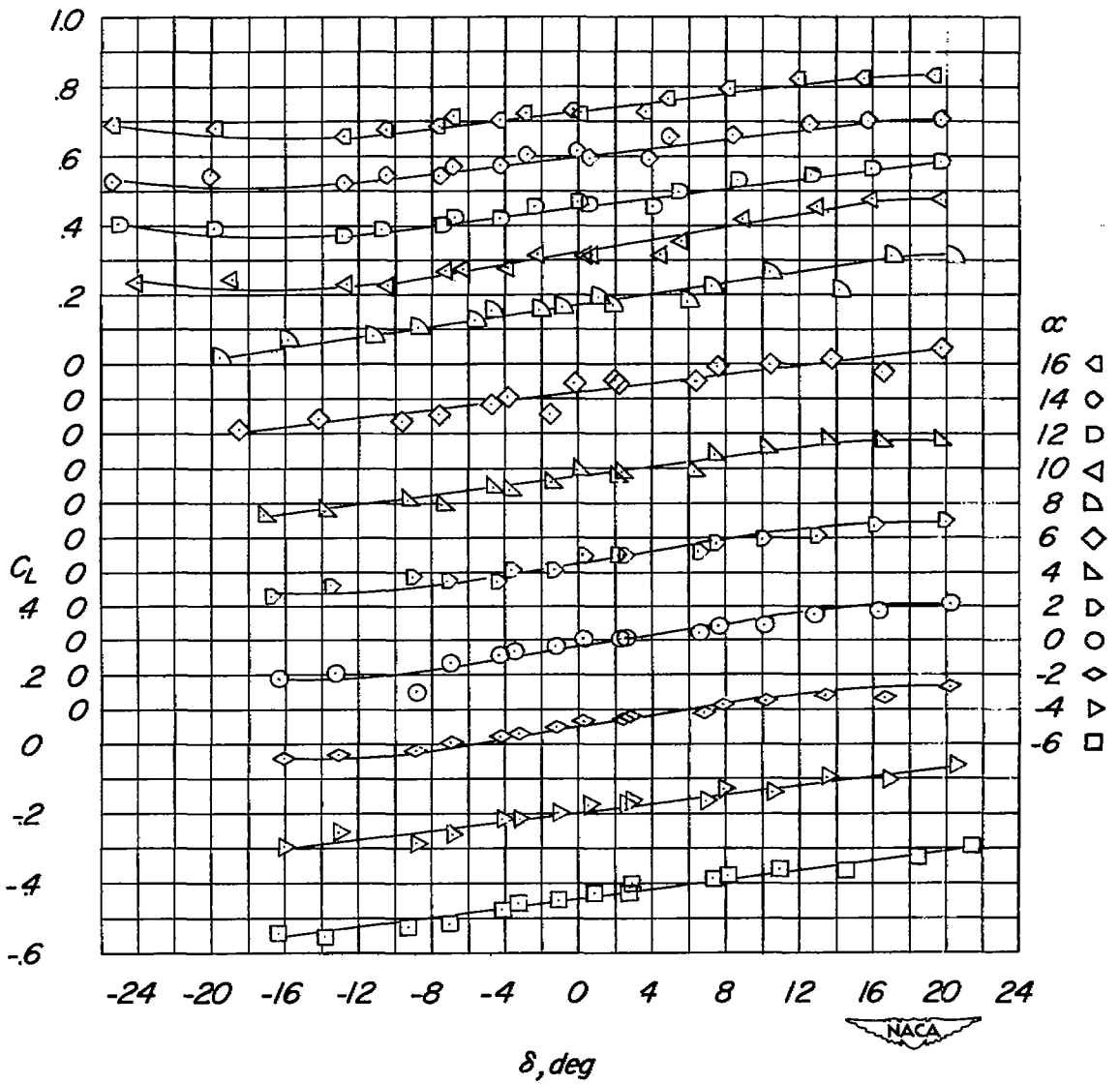

(d) M = 0.85.

Figure 6.- Continued.

[redacted]

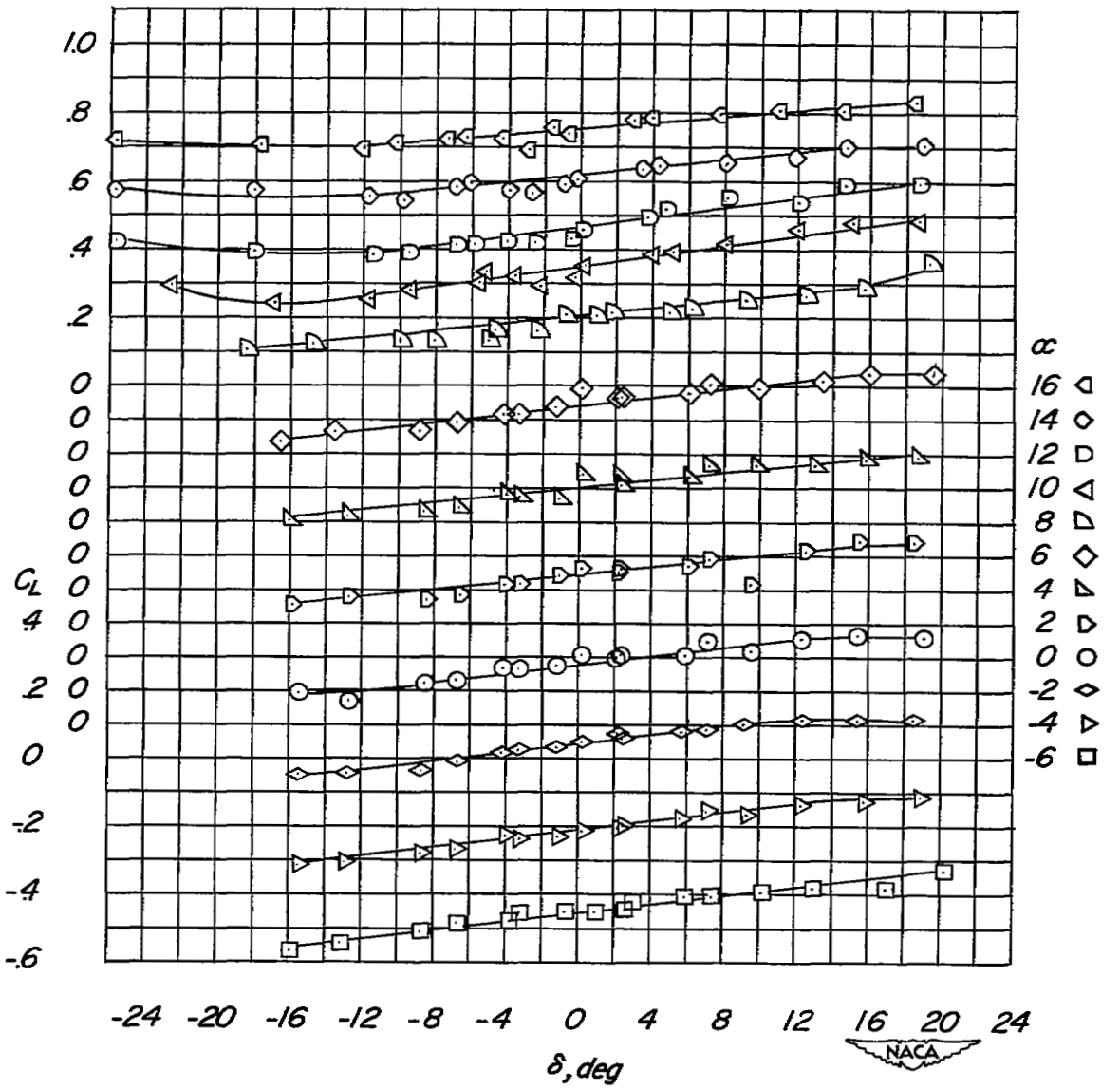

(e) M = 0.90.

Figure 6.- Continued.

[redacted]

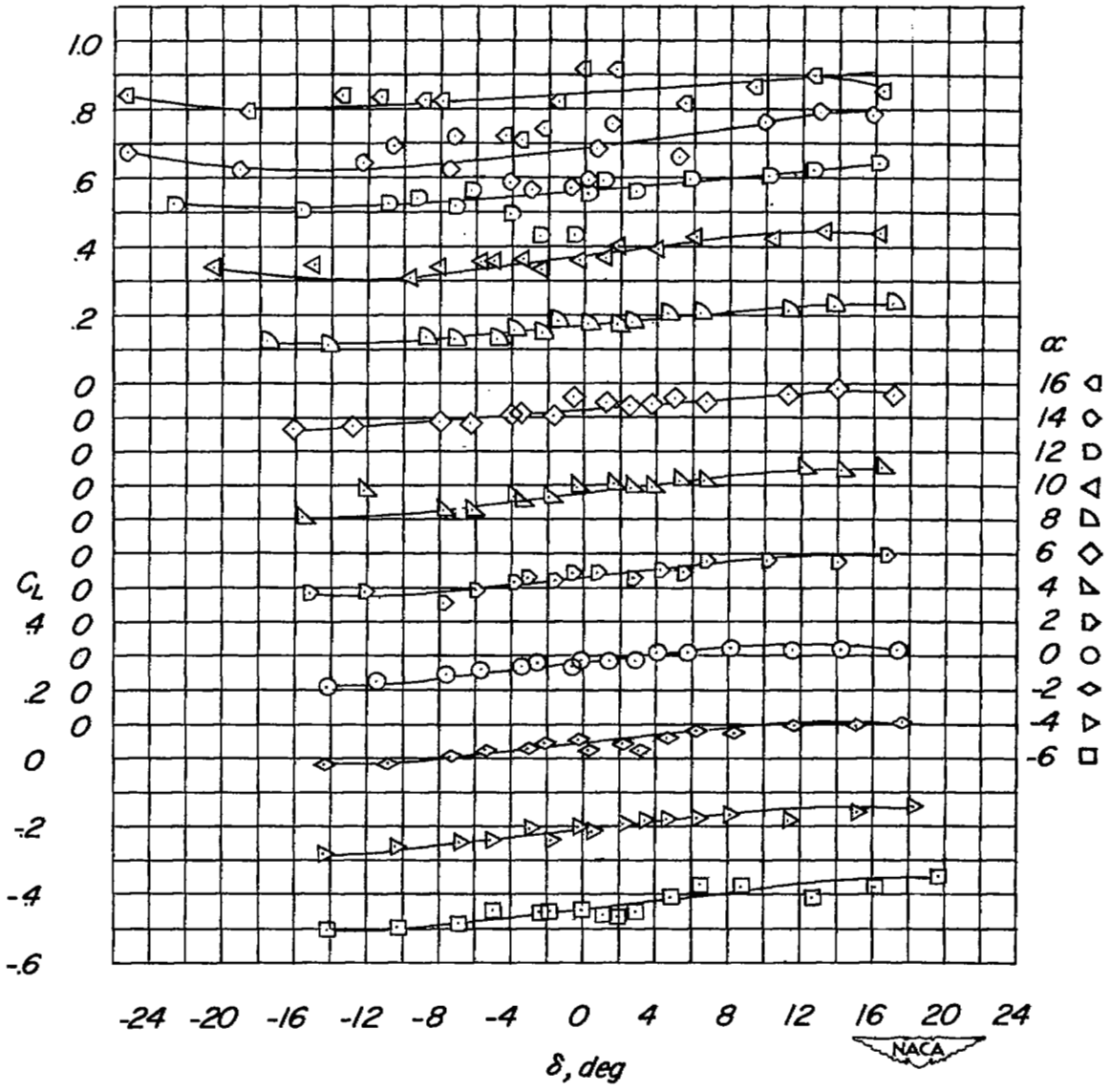

(f) M = 0.95.

Figure 6.- Continued.

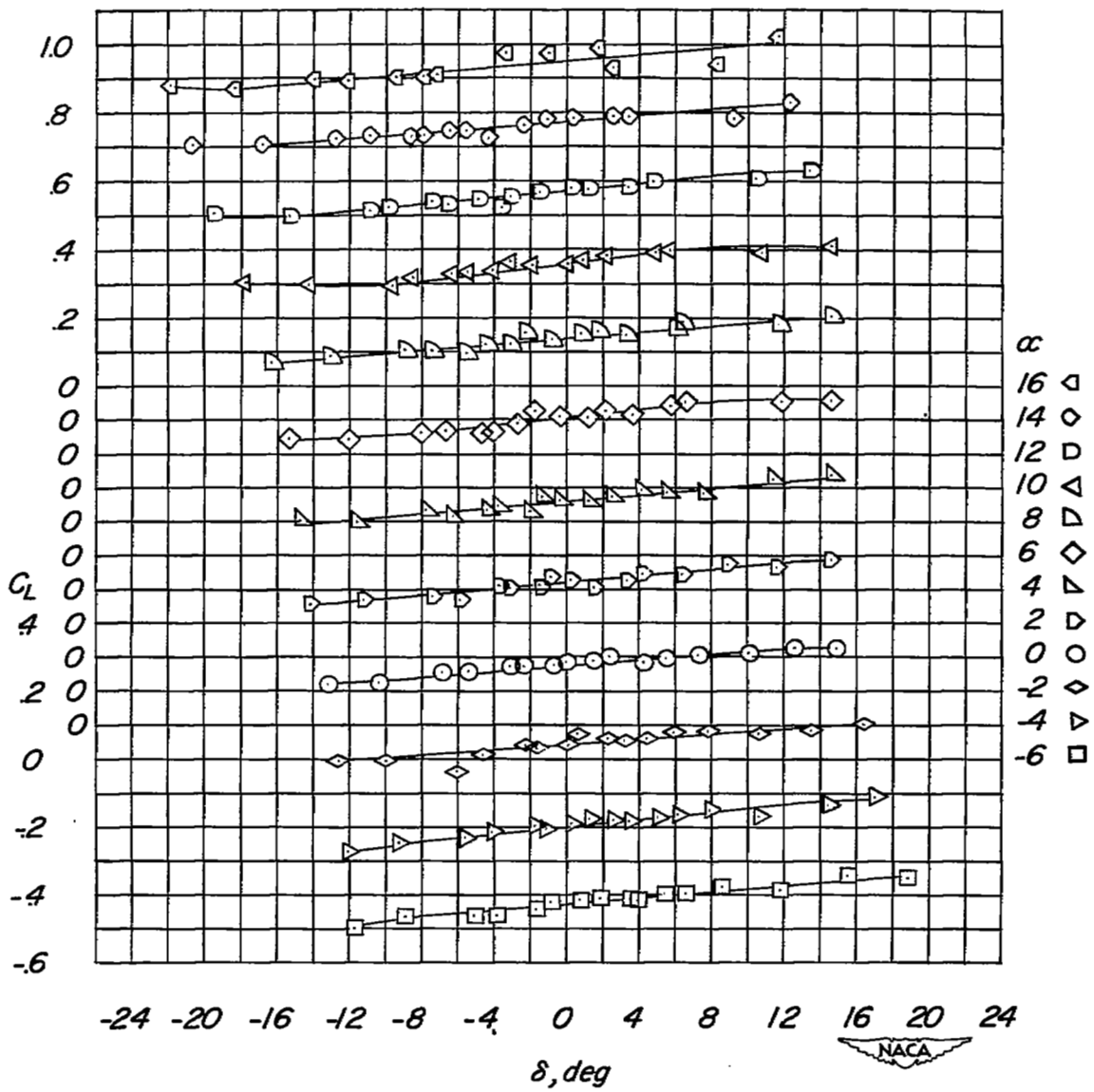

(g) M = 1.00.

Figure 6.- Continued.

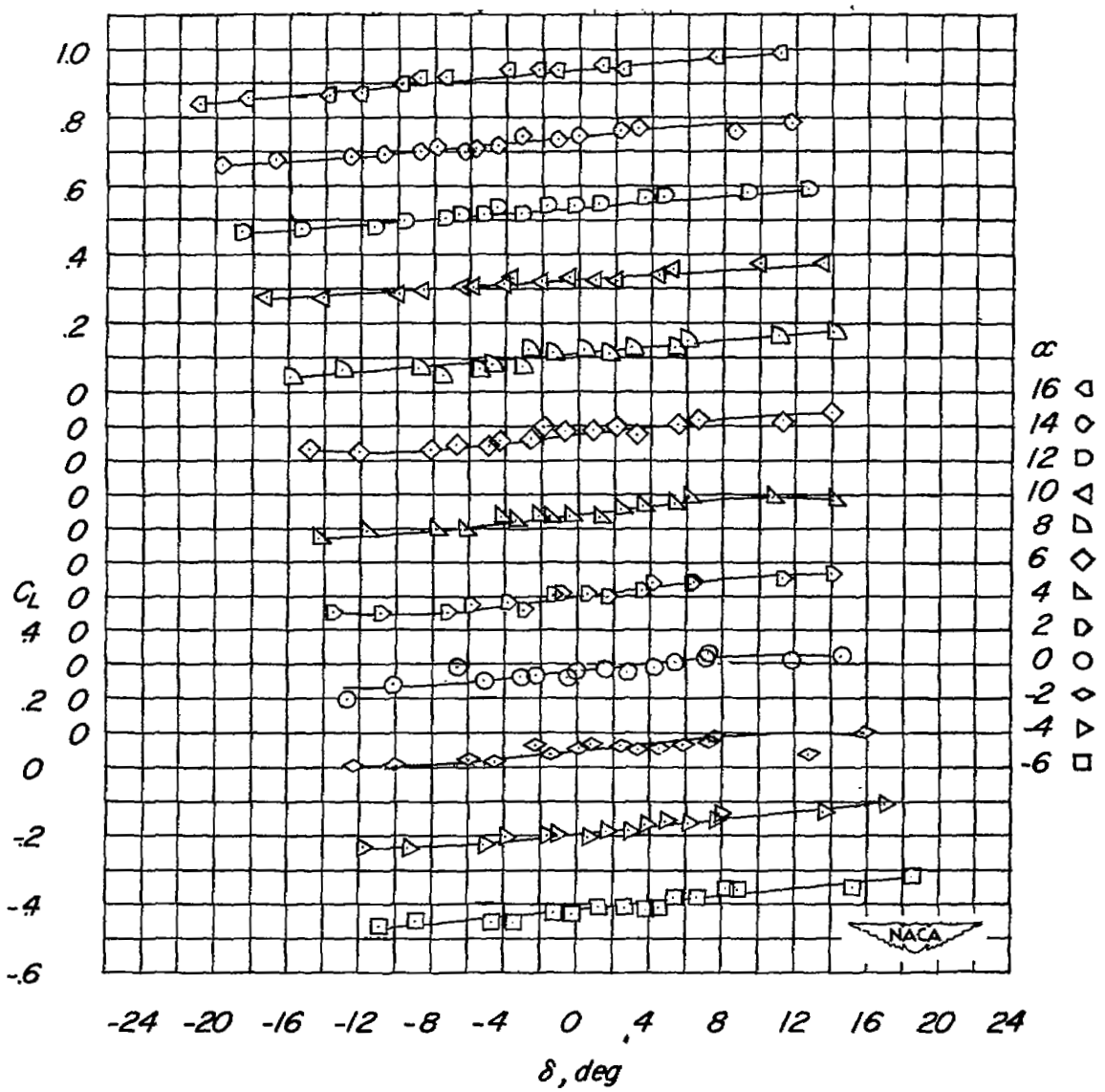

(h) M = 1.05.

Figure 6.- Continued.

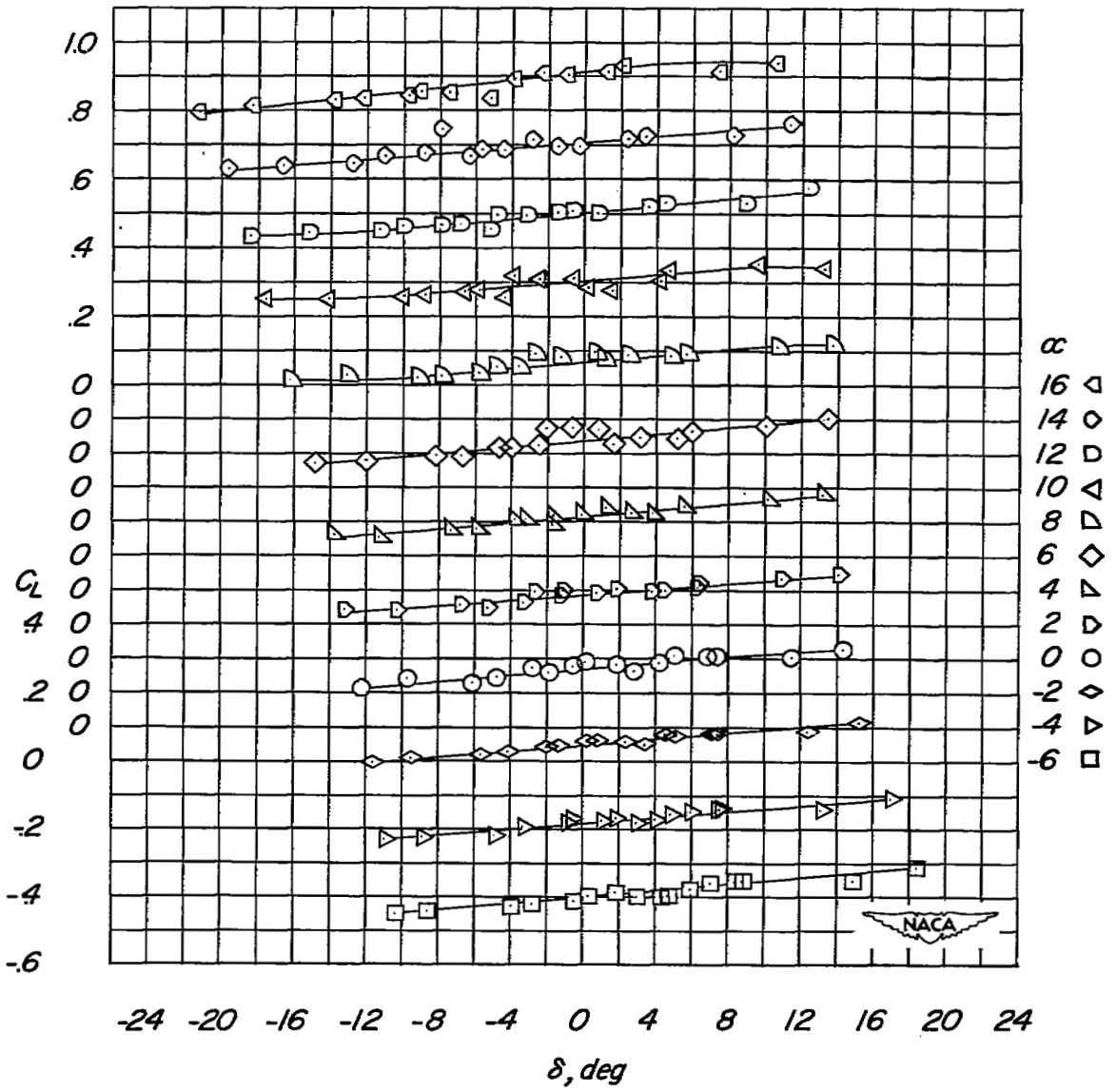

(i) M = 1.10.

Figure 6.- Concluded.

[redacted]

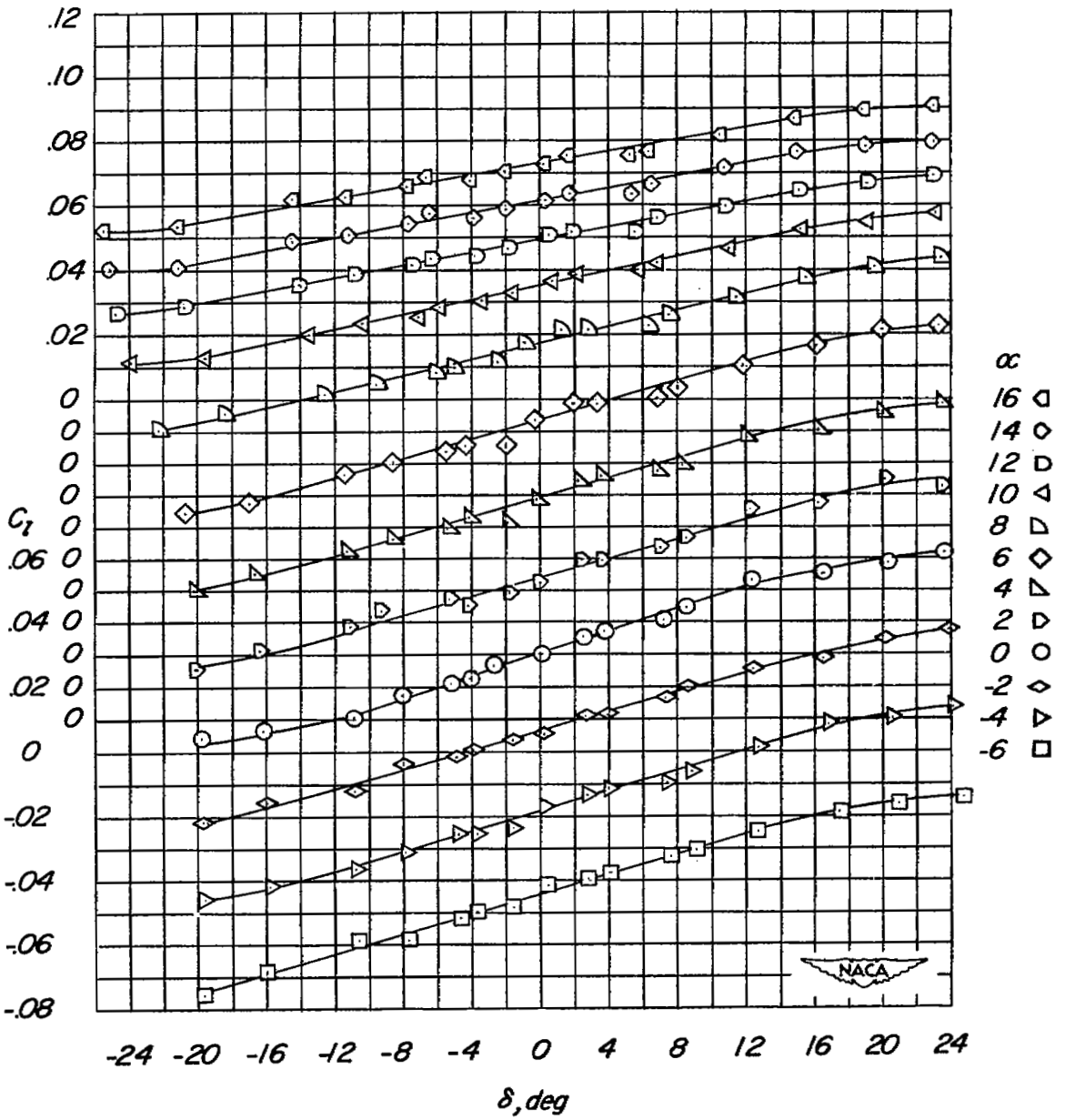

(a) M = 0.60.

Figure 7.- Variation of rolling-moment coefficient with control deflection for various angles of attack.

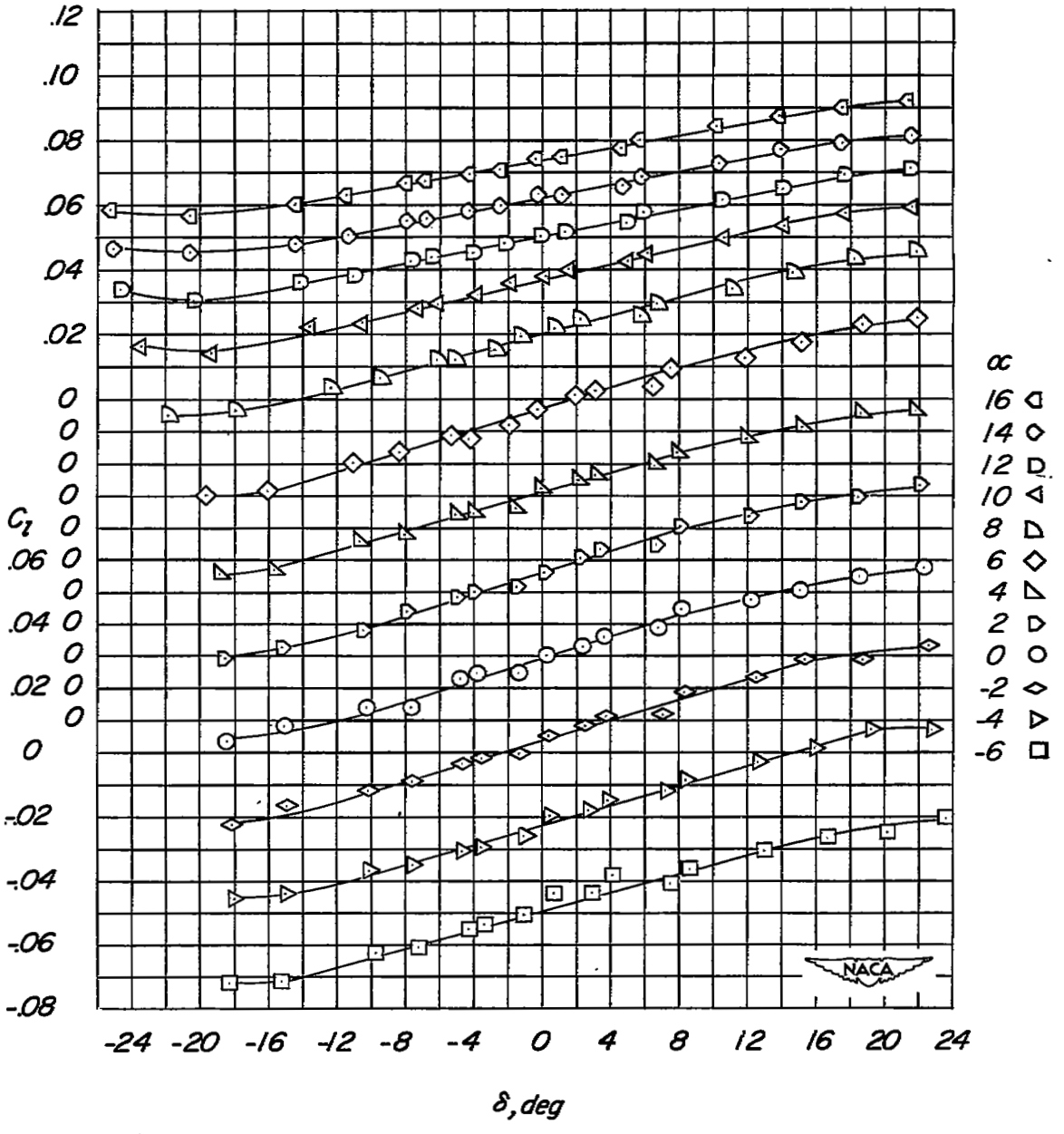

(b) M = 0.70.

Figure 7.- Continued.

[redacted]

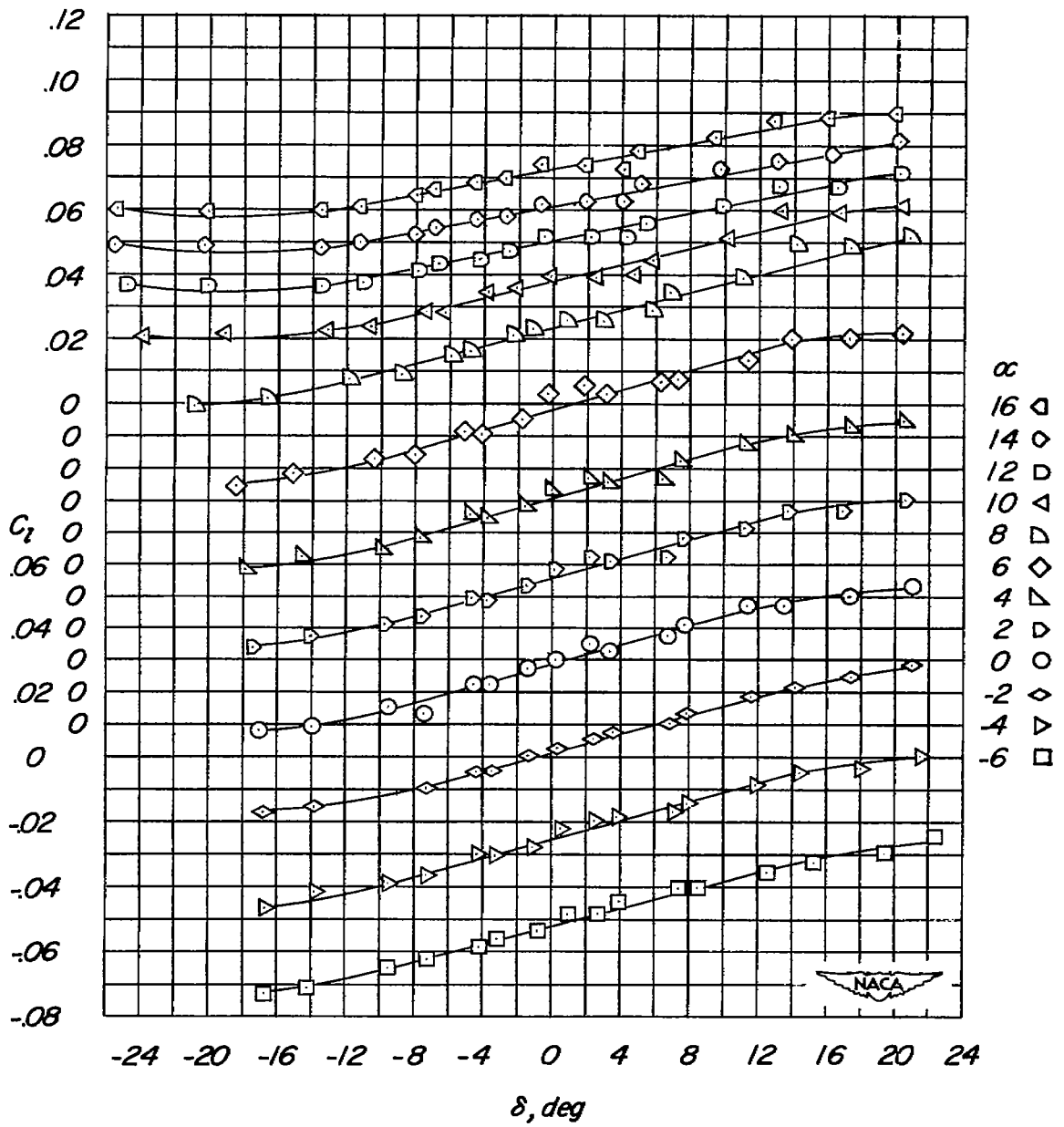

(c) M = 0.80.

Figure 7.- Continued.

[redacted]

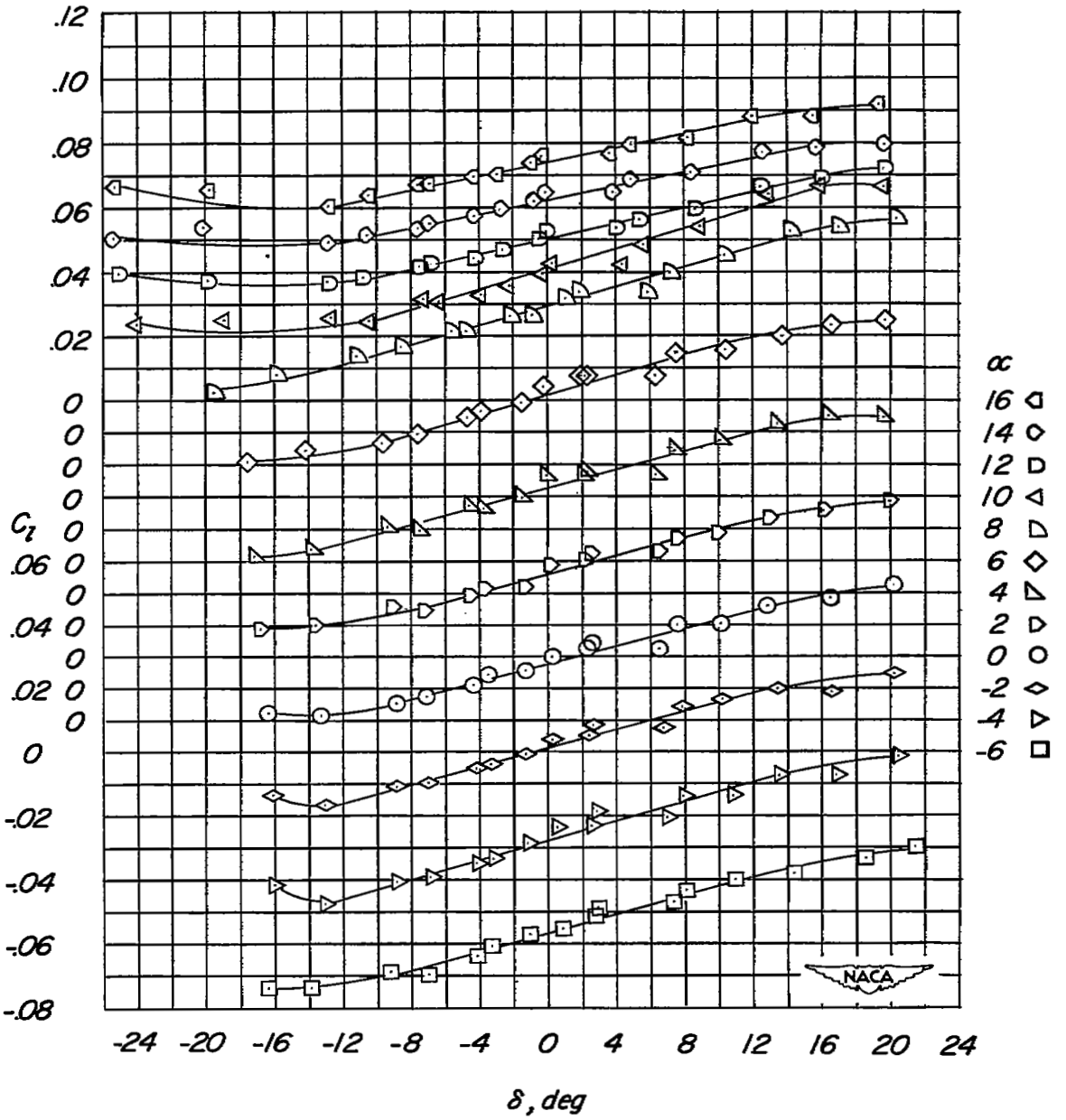

(d) M = 0.85.

Figure 7.- Continued.

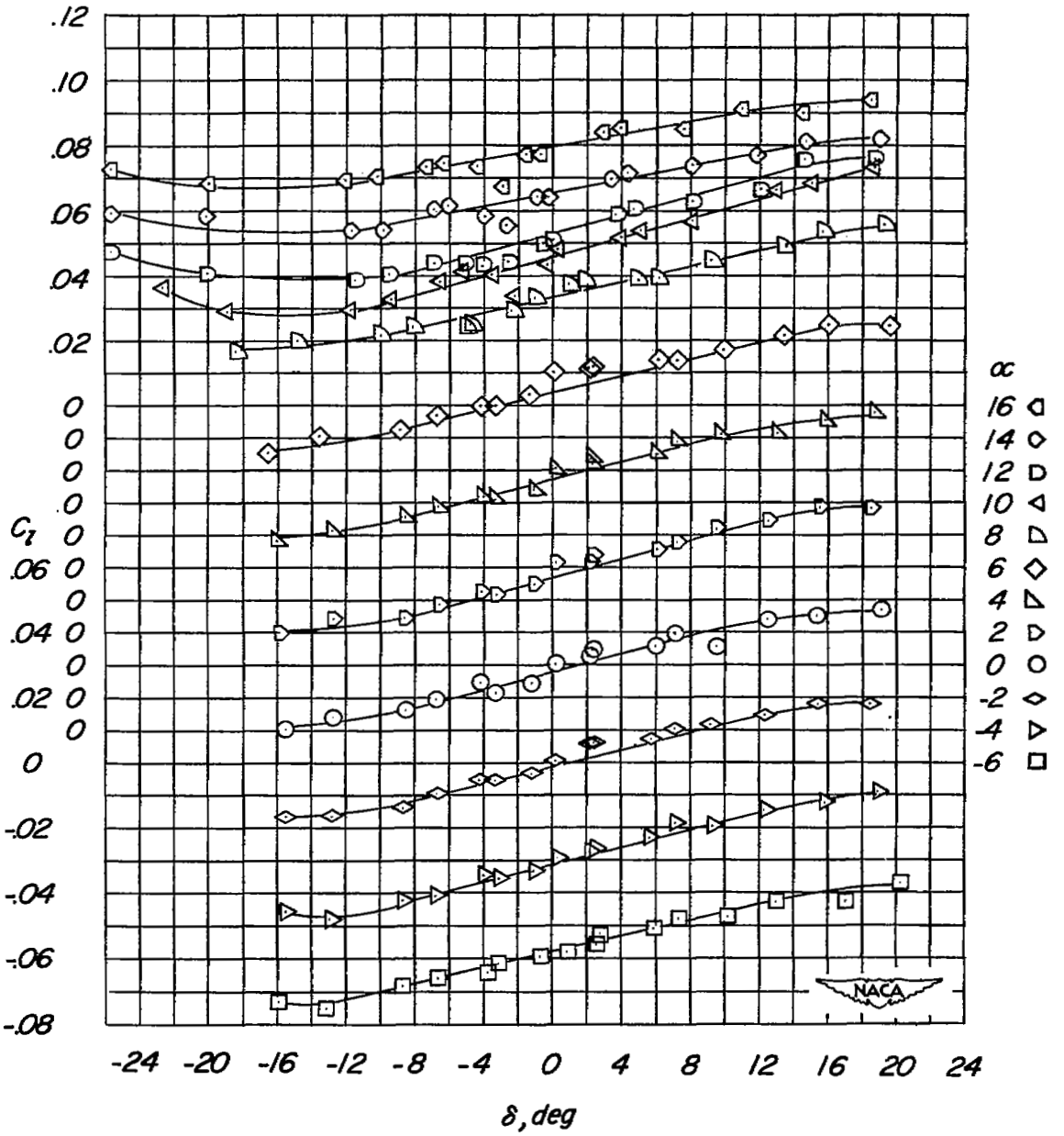

(e) M = 0.90.

Figure 7.- Continued.

[redacted]

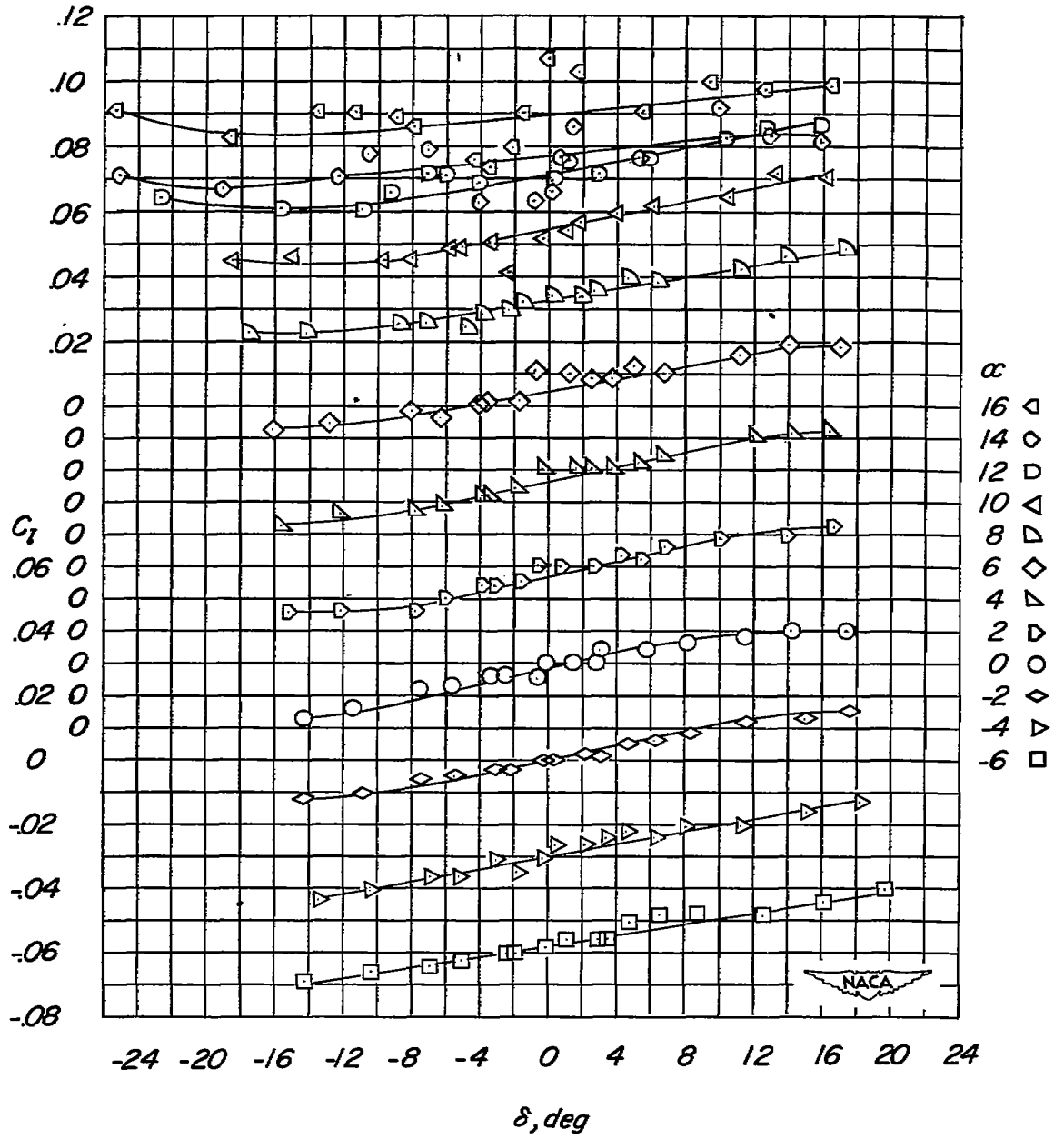

(f) M = 0.95.

Figure 7.- Continued.

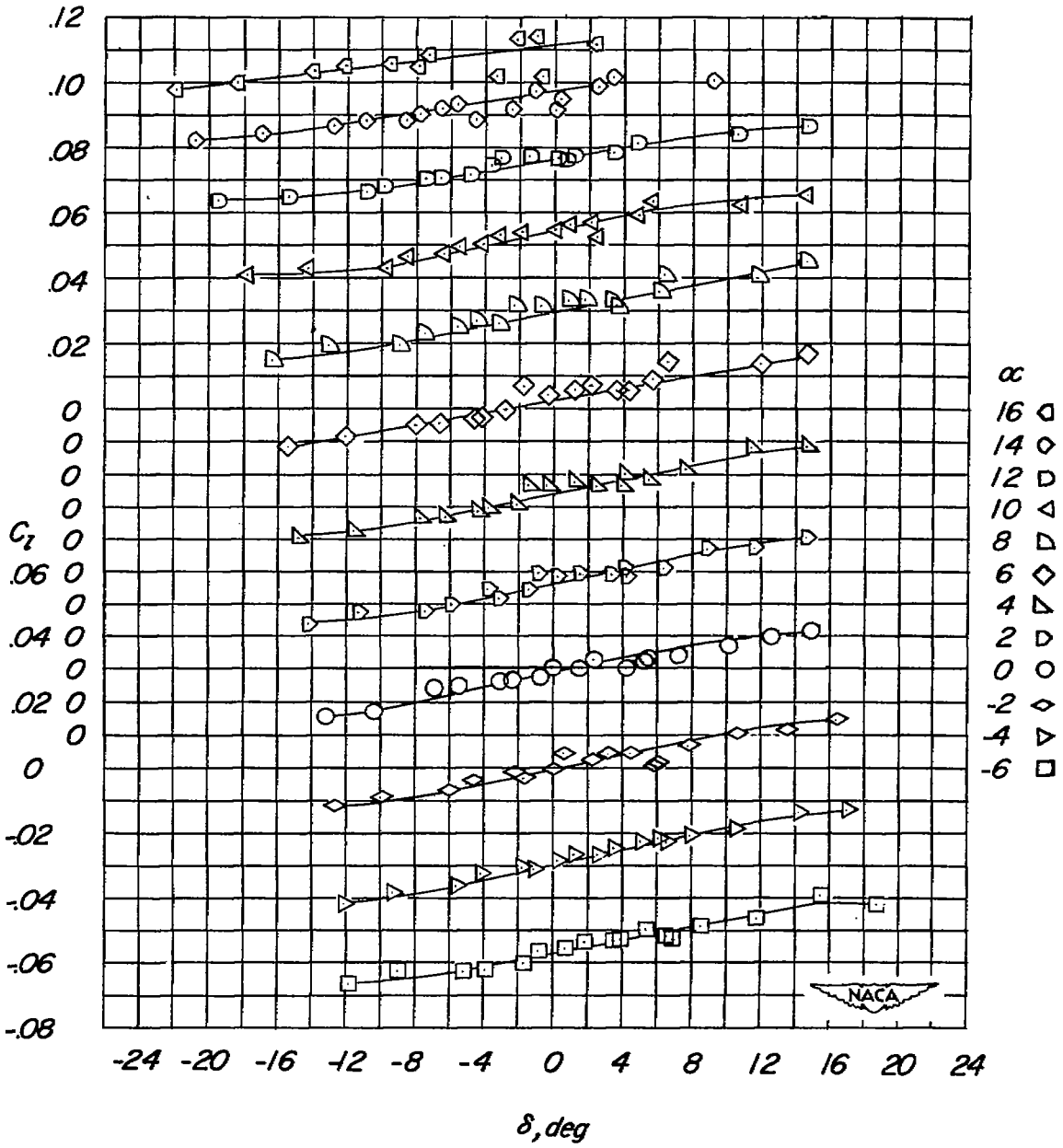

(g) M = 1.00.

Figure 7.- Continued.

[redacted]

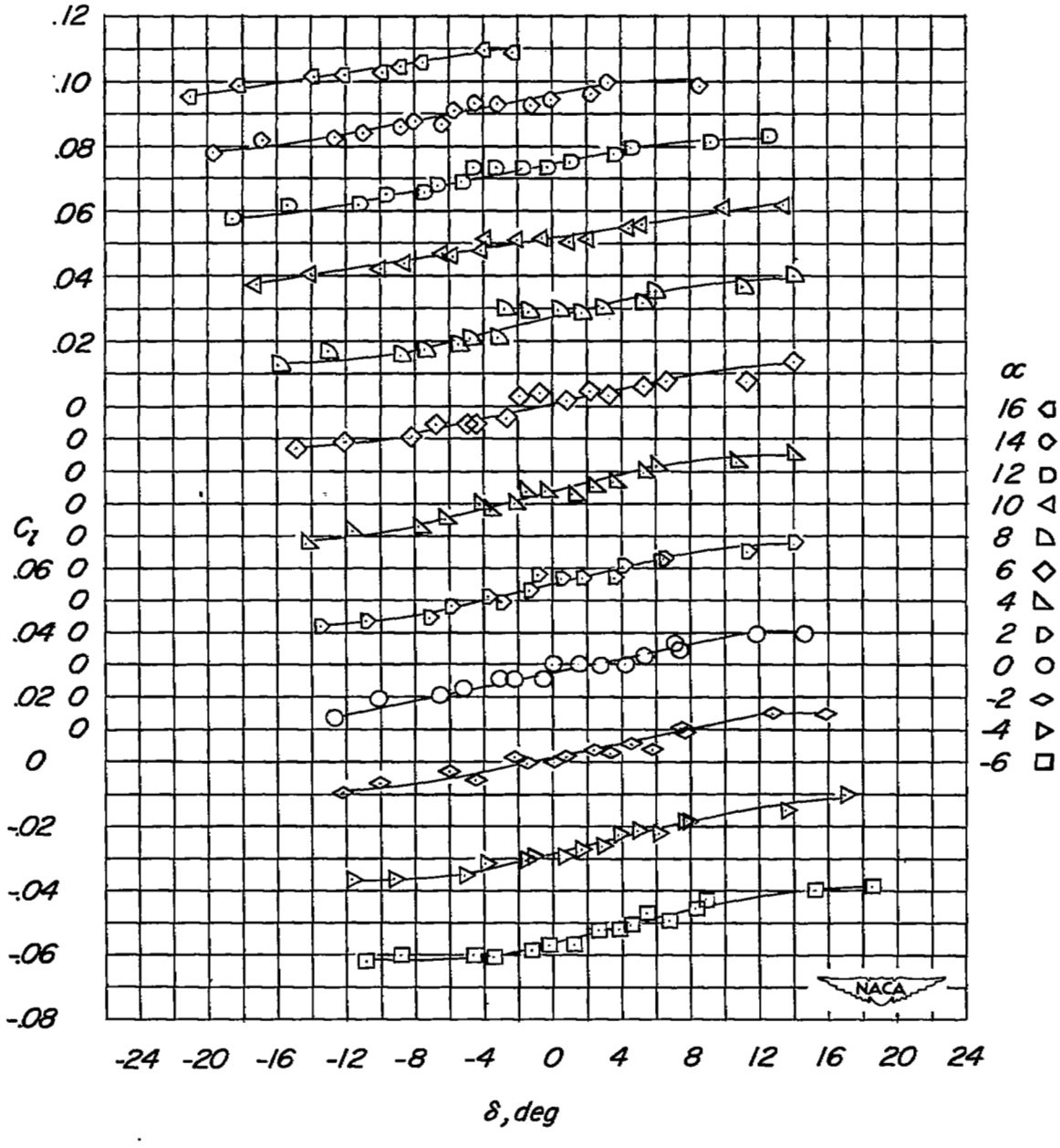

(h) M = 1.05.

Figure 7.- Continued.

[redacted]

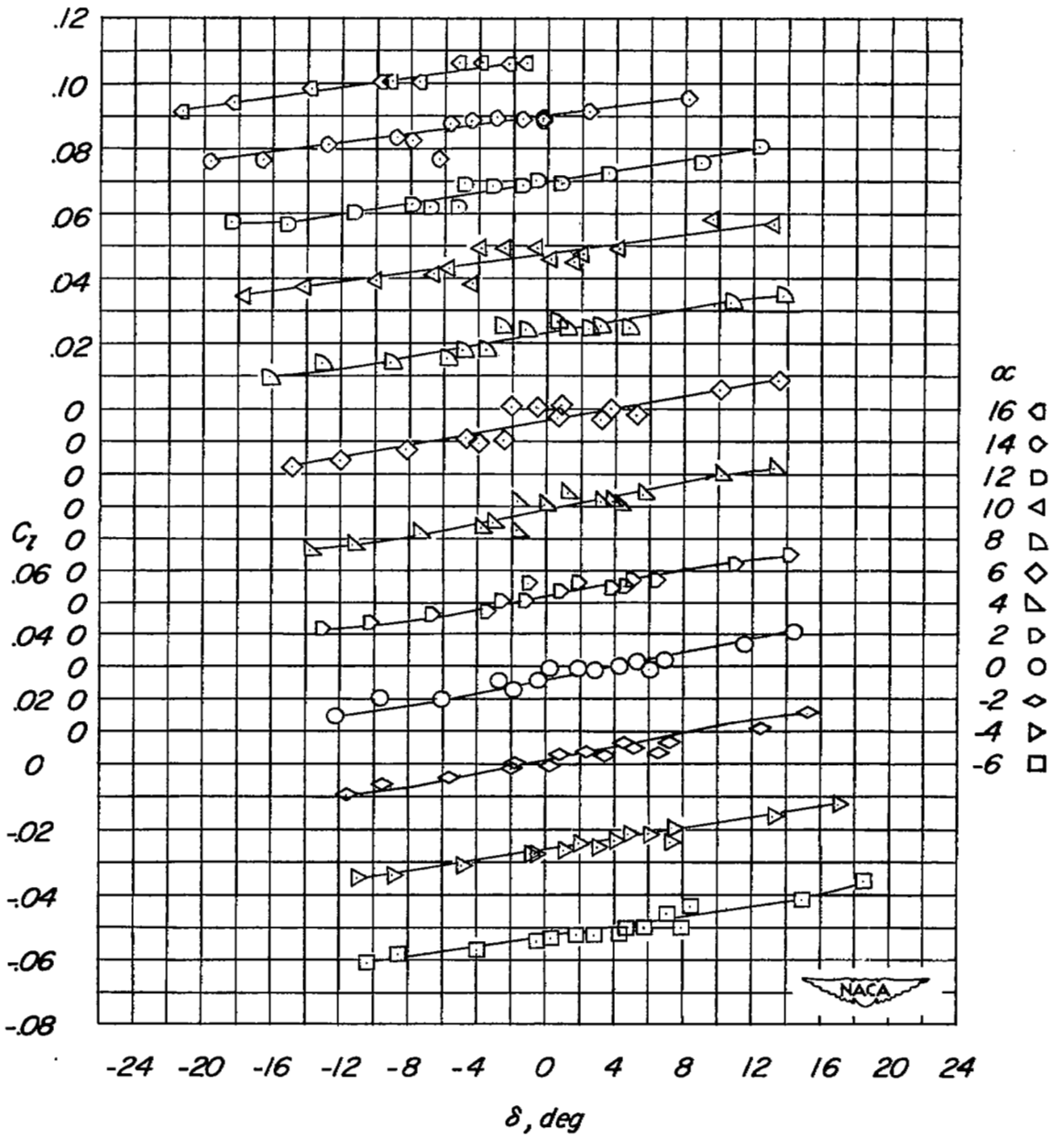

(i) M = 1.10.

Figure 7.- Concluded.

[redacted]

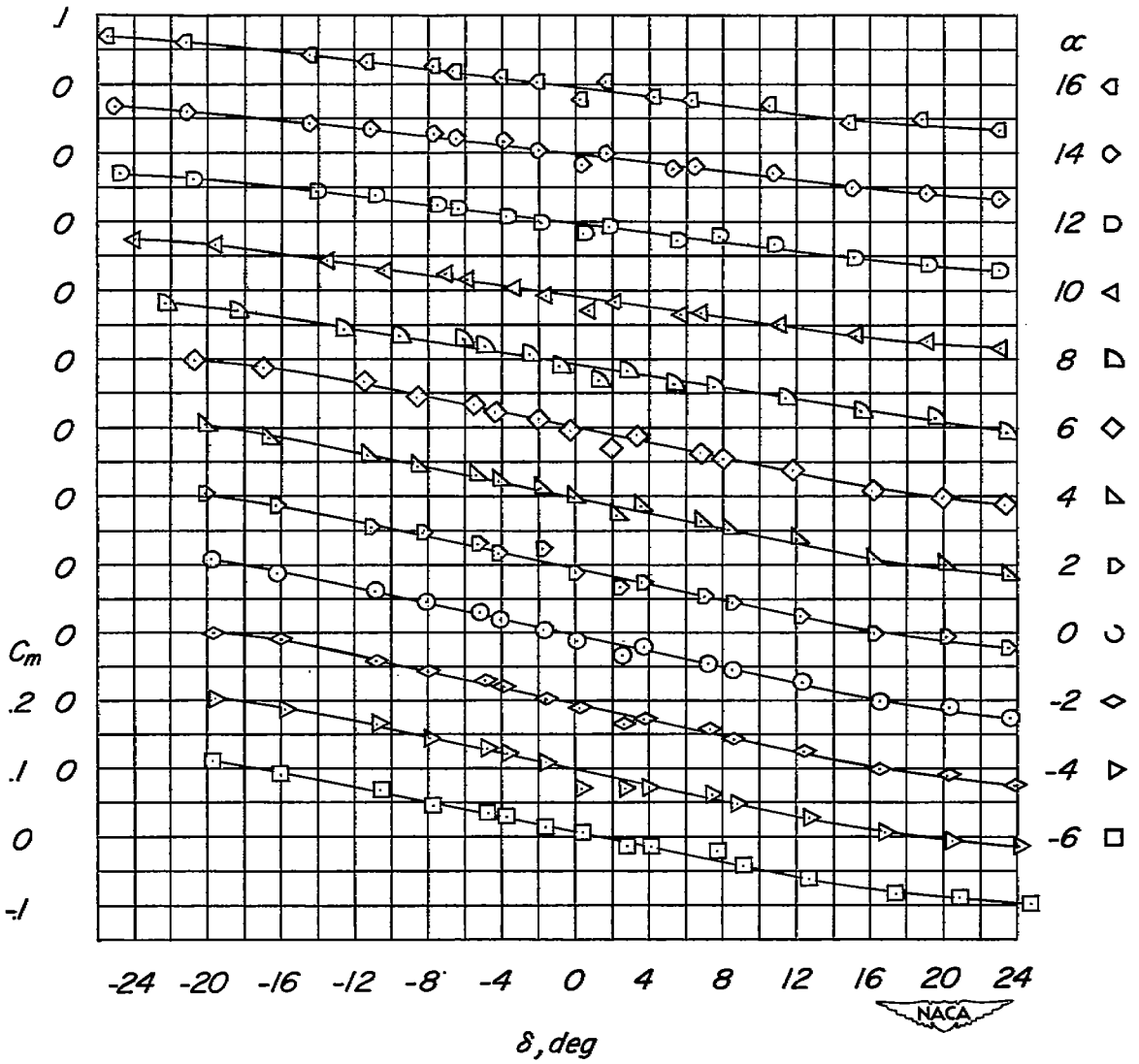

(a) M = 0.60.

Figure 8.- Variation of pitching-moment coefficient with control deflection for various angles of attack.

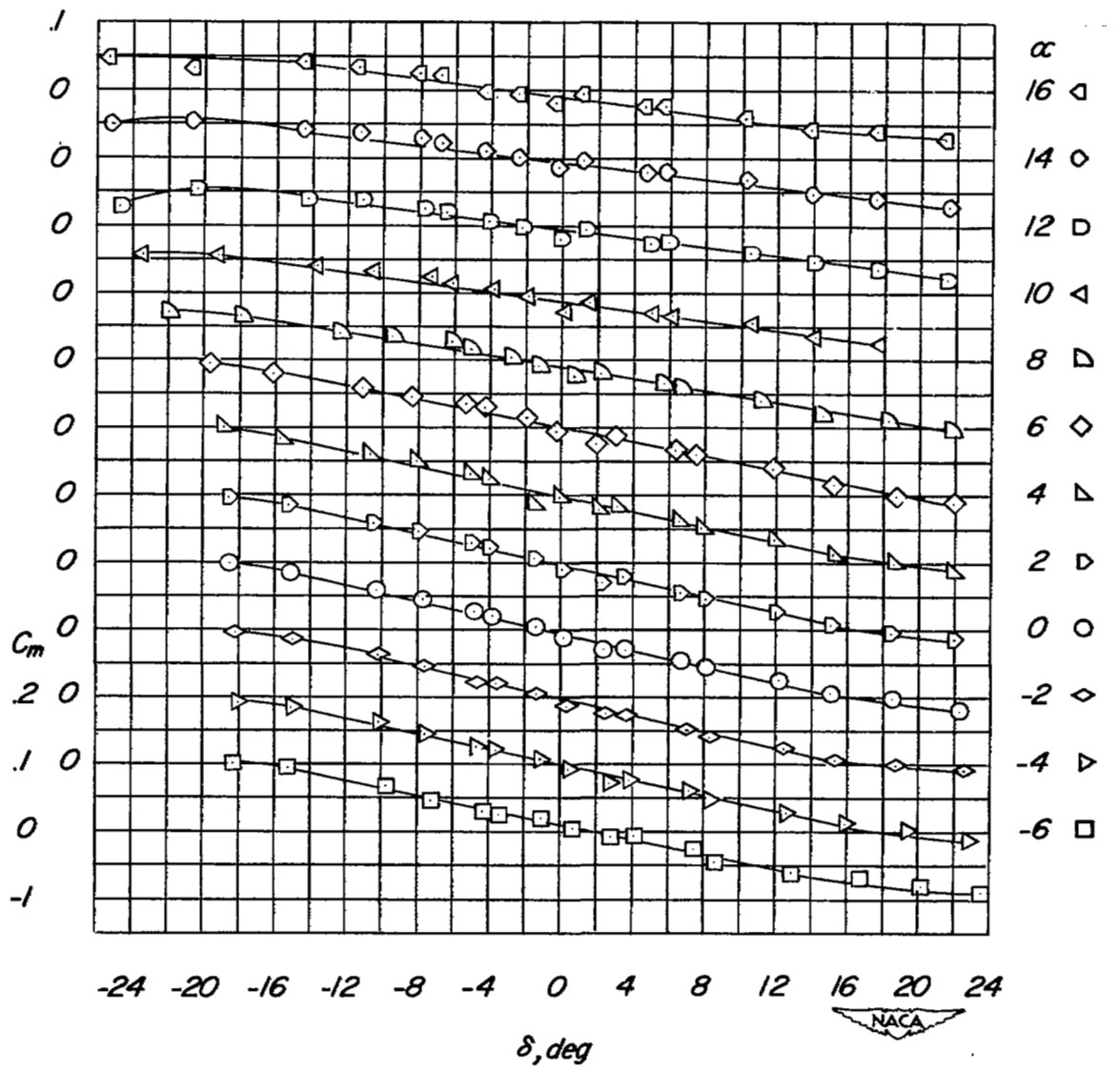

(b) M = 0.70.

Figure 8.- Continued.

[redacted]

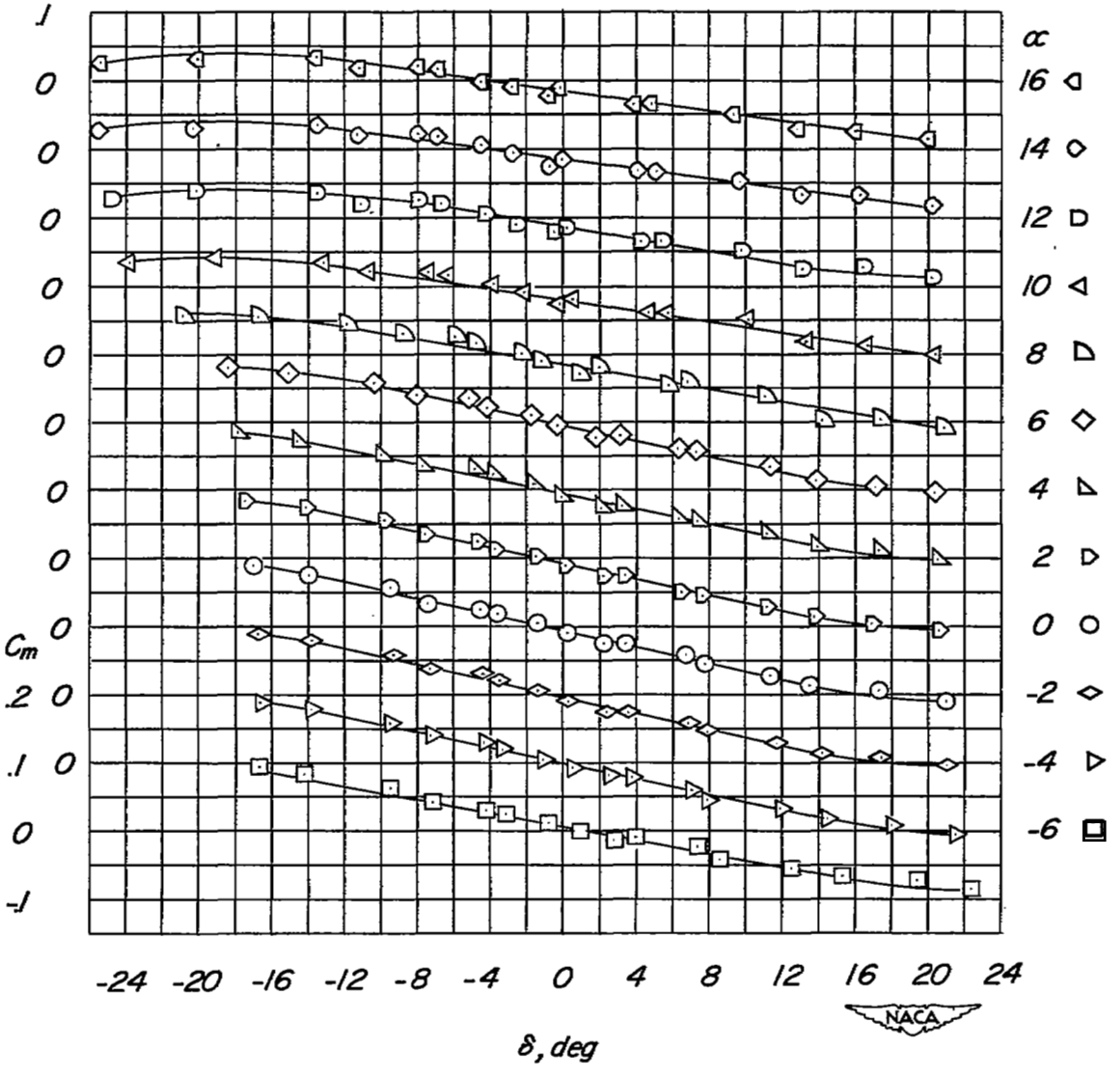

(c) M = 0.80.

Figure 8.- Continued.

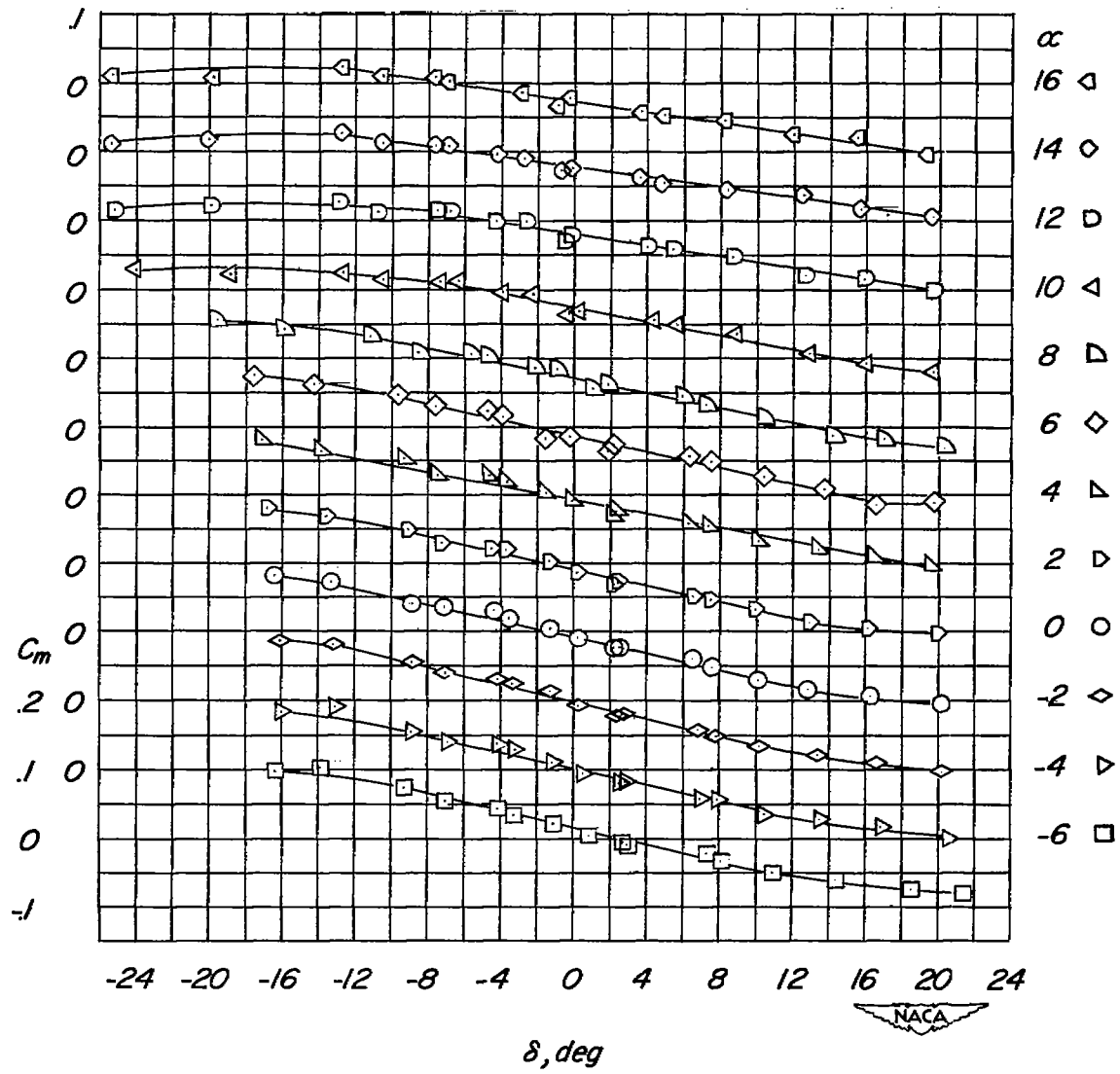

(d) M = 0.85.

Figure 8.- Continued.

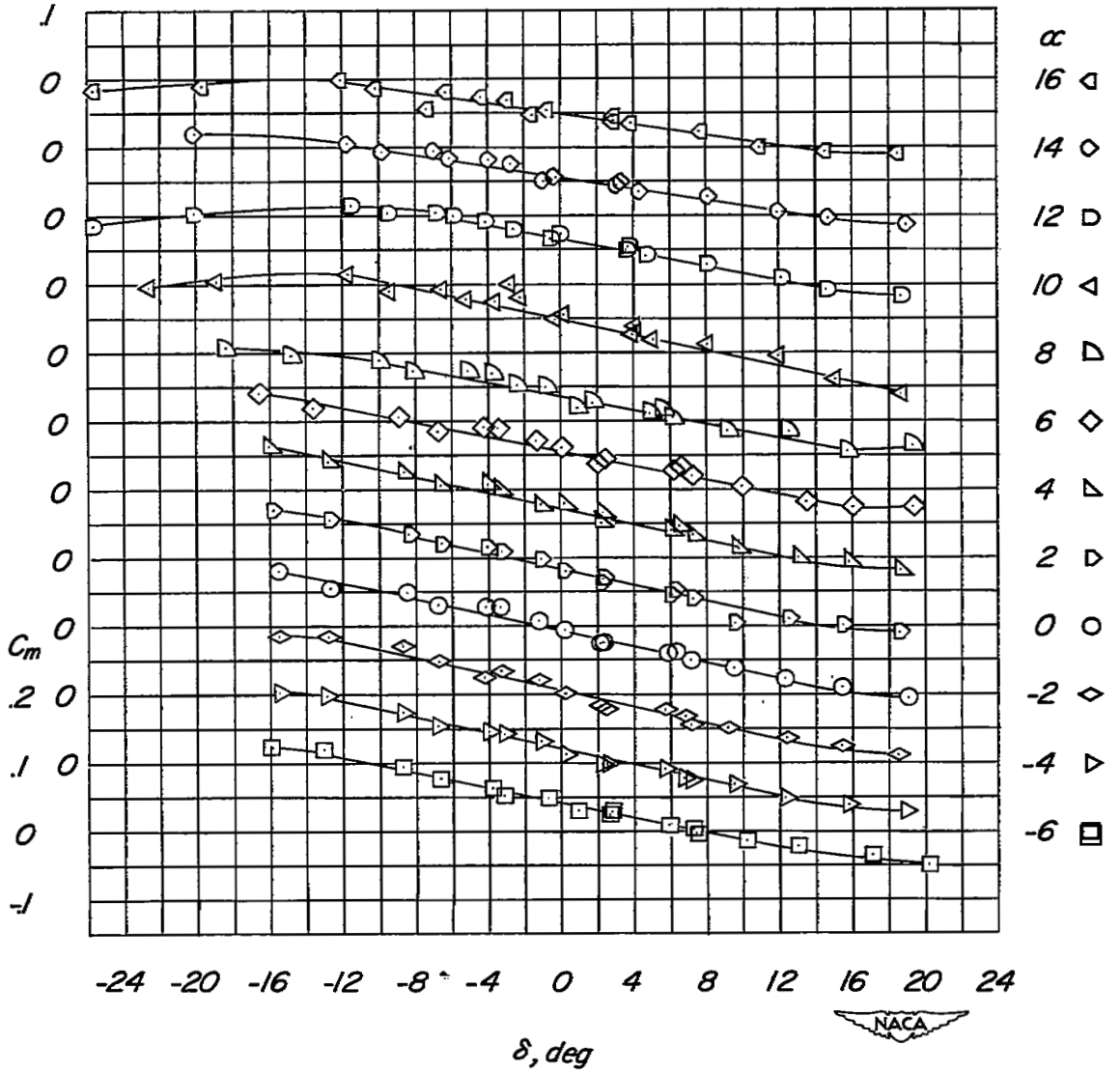

(e) M = 0.90.

Figure 8.- Continued.

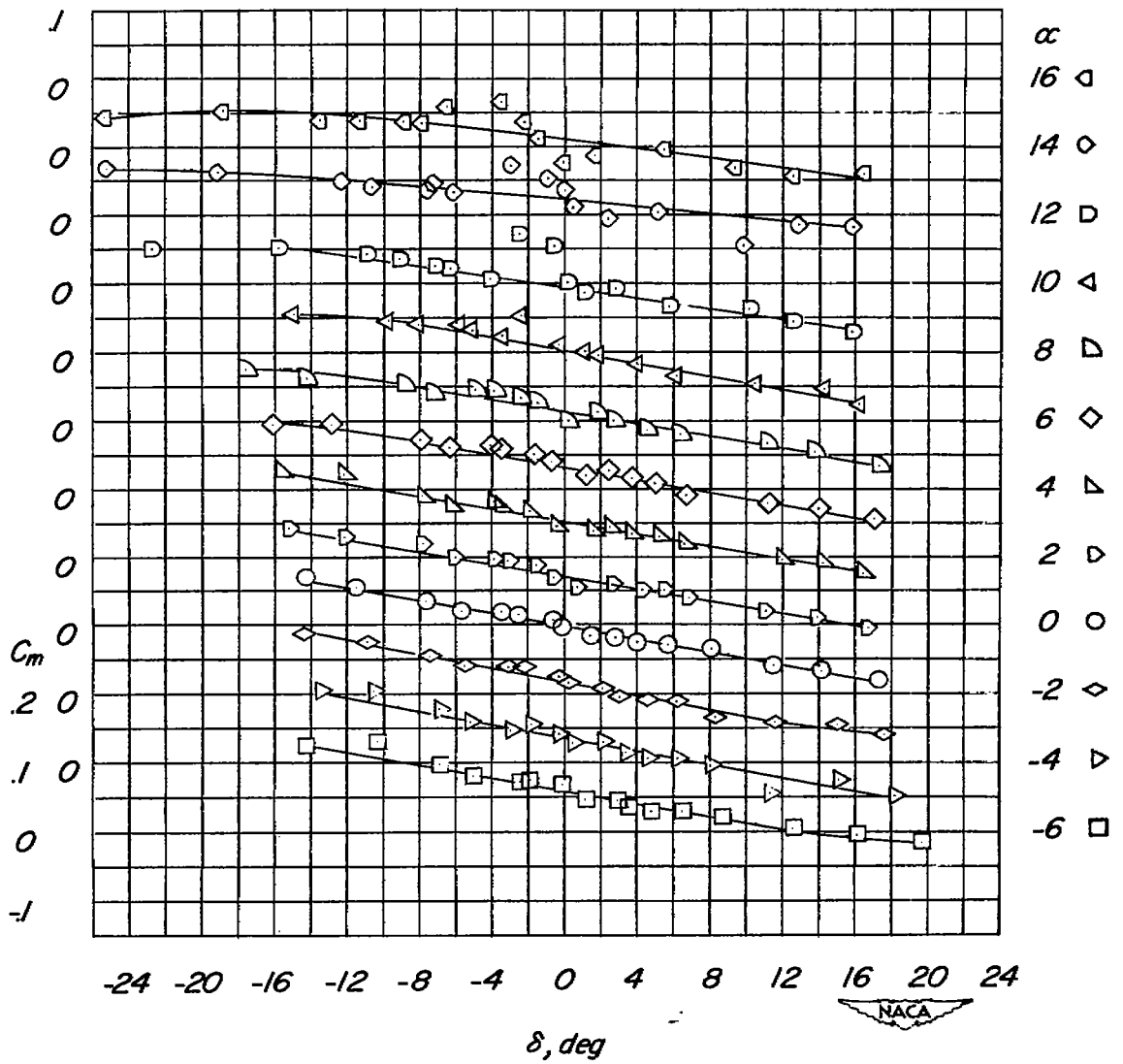

(f) M = 0.95.

Figure 8.- Continued.

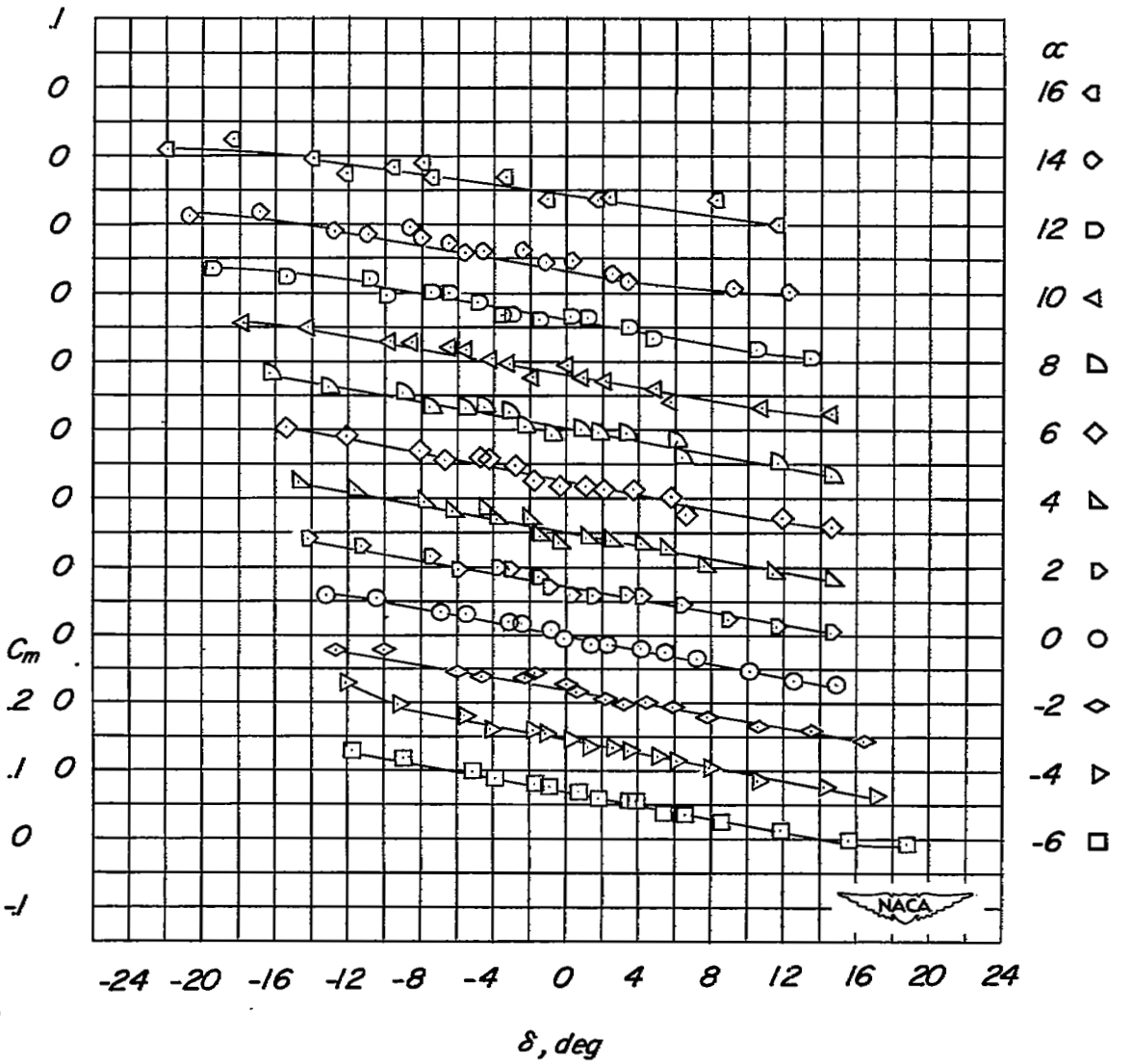

(g) M = 1.00.

Figure 8.- Continued.

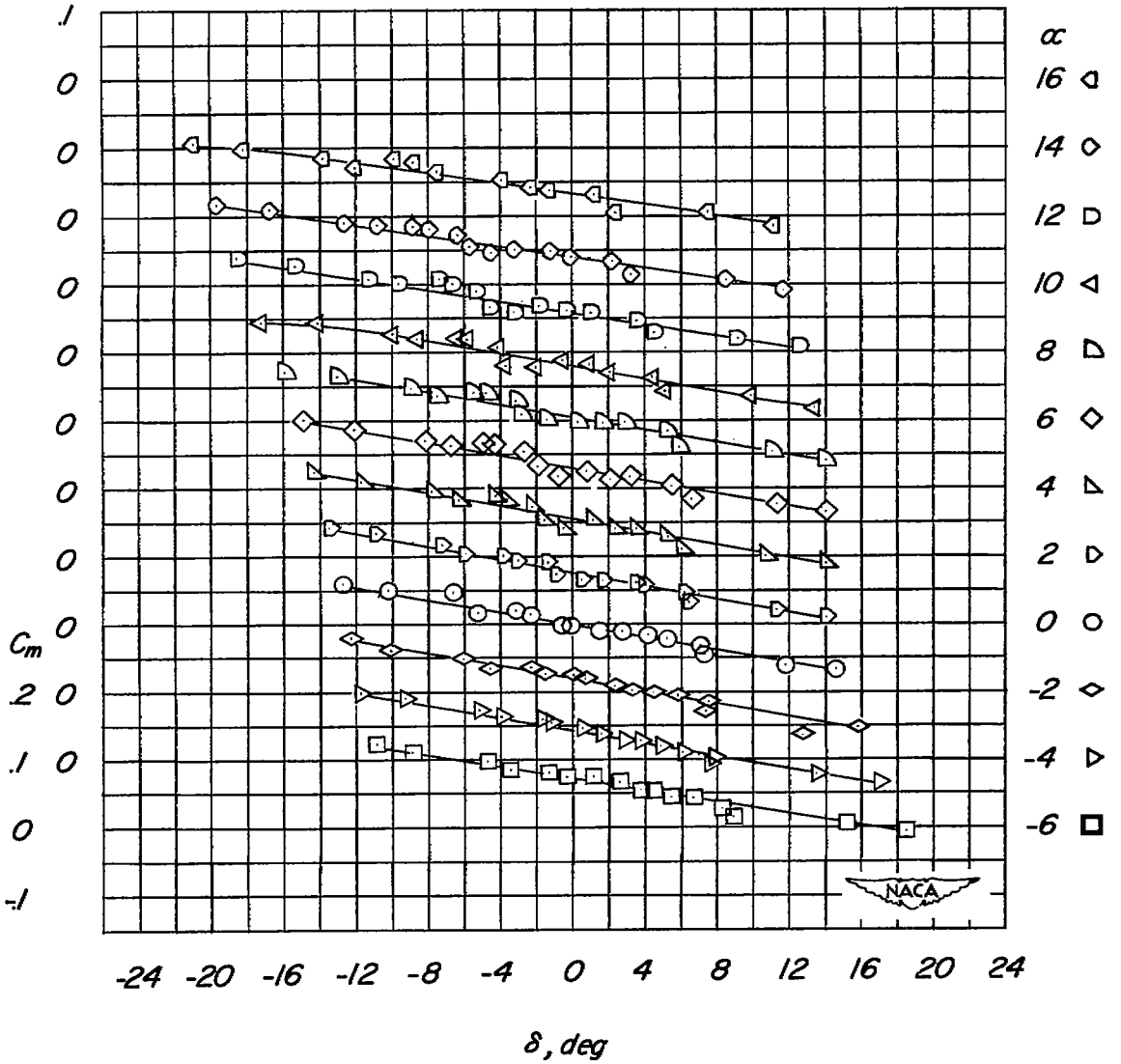

(h) M = 1.05.

Figure 8.- Continued.

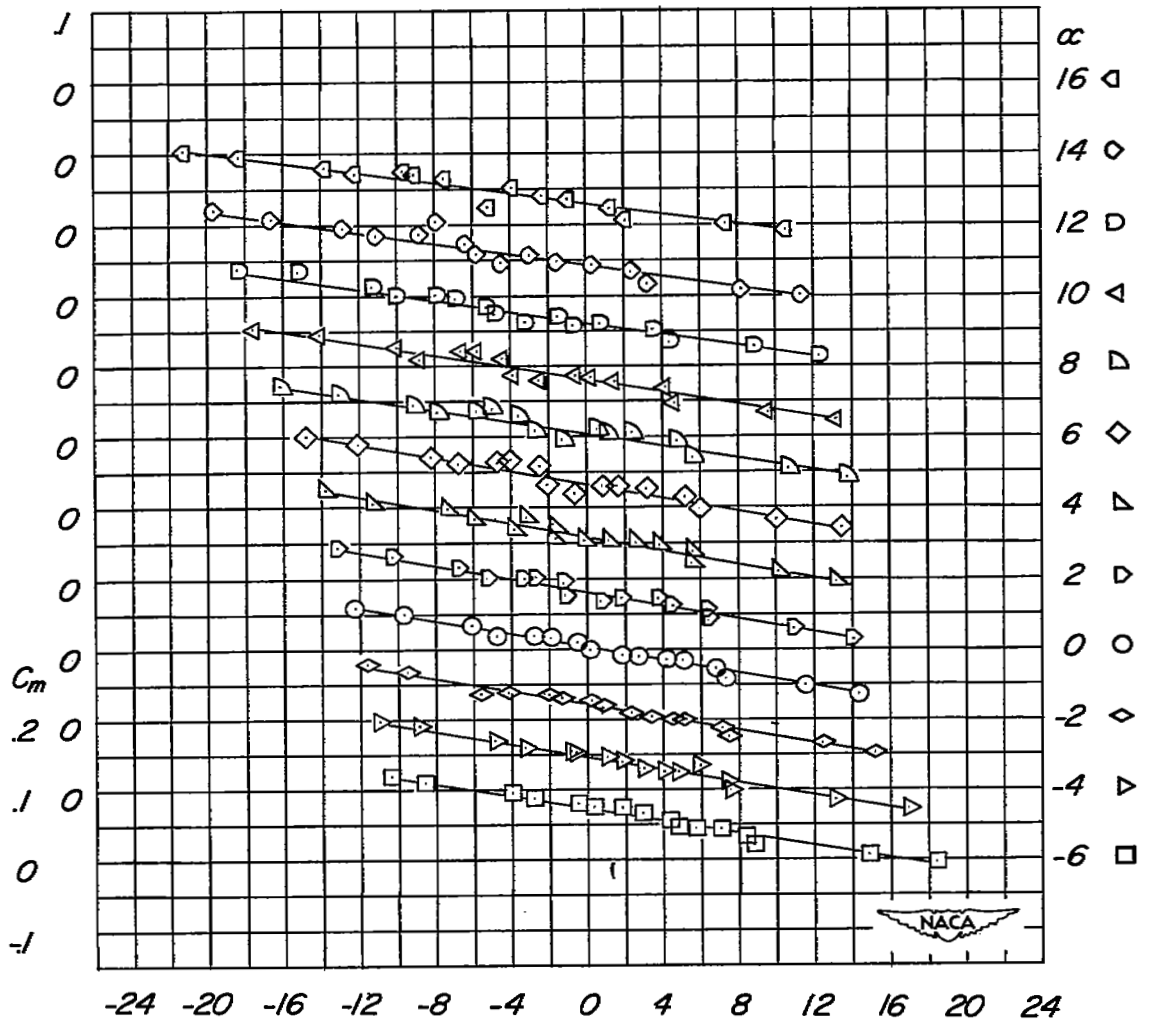

(i) M = 1.10.

Figure 8.- Concluded.

[redacted]

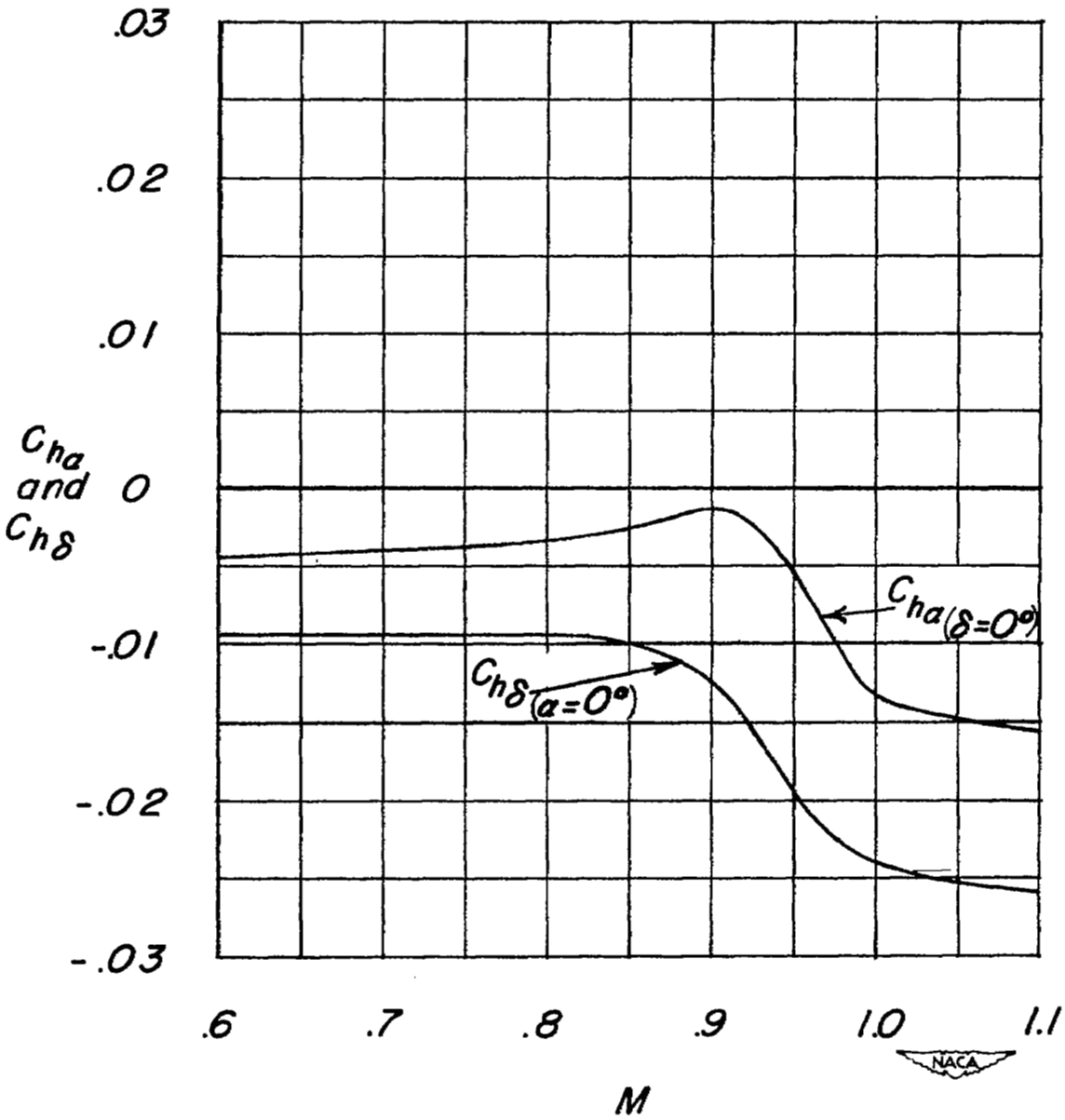

Figure 9.- Variation of the hinge-moment parameters C_{h_α} and C_{h_δ} with Mach number.

[redacted]

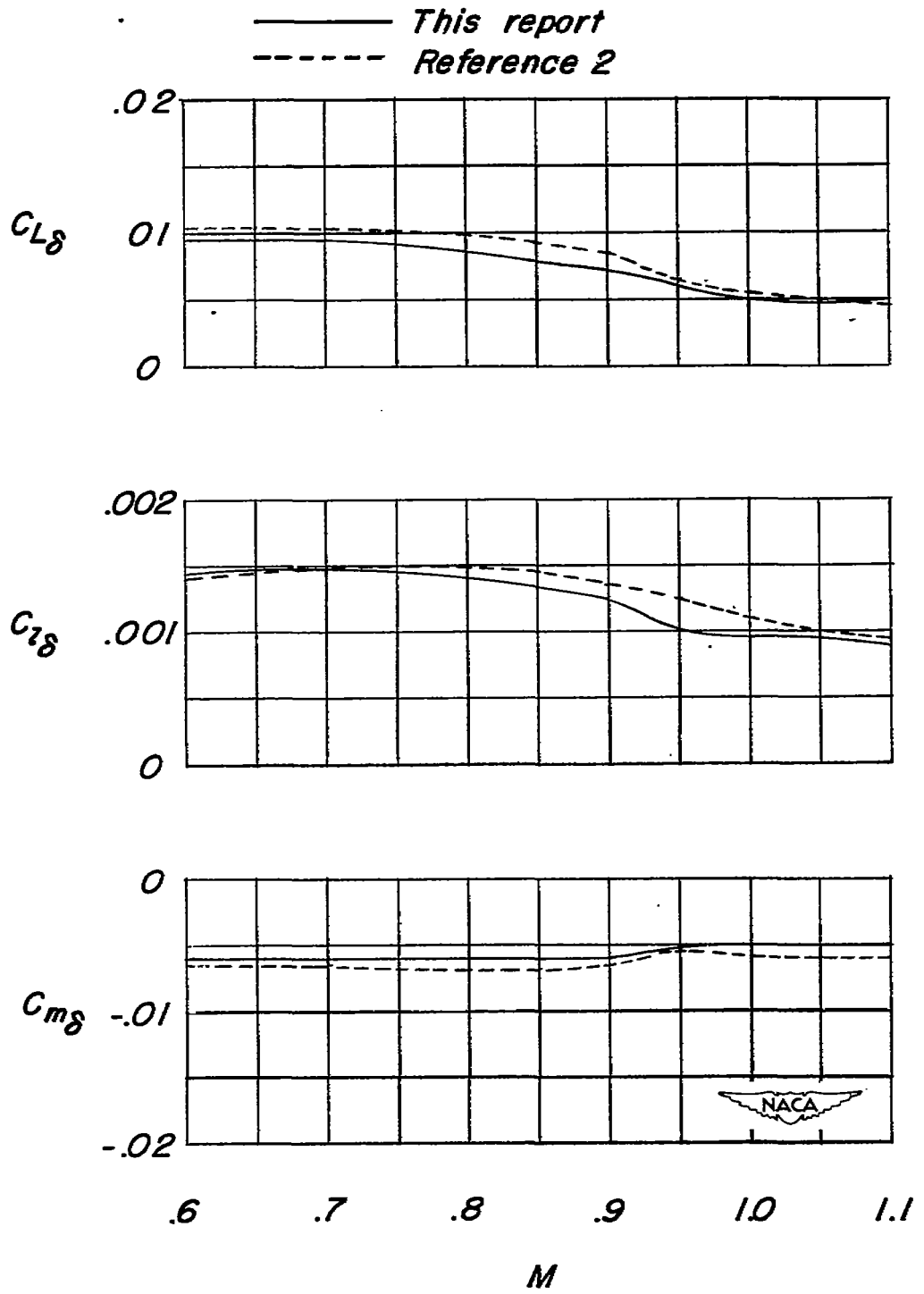

Figure 10.- Variation of the parameters C_{l_δ}, C_{L_δ}, and C_{m_δ} with Mach number. $\alpha = 0^\circ$.

[redacted]

[redacted]